Karst spring discharge modeling based on deep learning using spatially distributed input data

Andreas Wunsch[1], Tanja Liesch[1], Guillaume Cinkus[2], Nataša Ravbar[3], Zhao Chen[4], Naomi Mazzilli[5], Hervé Jourde[2], and Nico Goldscheider[1]

[1]Karlsruhe Institute of Technology (KIT), Institute of Applied Geosciences, Hydrogeology, Kaiserstr. 12, 76131 Karlsruhe, Germany
[2]HydroSciences Montpellier (HSM), Université de Montpellier, CNRS, IRD, 34090 Montpellier, France
[3]ZRC SAZU, Karst Research Institute, Titov trg 2, 6230 Postojna, Slovenia
[4]Environmental Resources Management, Siemensstr. 9, 63263 Neu-Isenburg, Germany
[5]UMR 1114 EMMAH (AU-INRAE), Université d'Avignon, 84000 Avignon, France

Correspondence: Andreas Wunsch (andreas.wunsch@kit.edu)

Abstract. Despite many existing approaches, modeling karst water resources remains challenging and often requires solid system knowledge. Artificial Neural Network approaches offer a convenient solution by establishing a simple input-output relationship on their own. However, in this context, temporal and especially spatial data availability is often an important constraint, as usually no or few climate stations within a karst spring catchment are available. Hence spatial coverage is often unsatis-
5 fying and can introduce severe uncertainties. To ~~avoid~~ overcome these problems, we use 2D-Convolutional Neural Networks (CNN) to directly process gridded meteorological data followed by a 1D-CNN to perform karst spring discharge simulation. We investigate three karst spring catchments in the Alpine and Mediterranean region with different meteorologic-hydrological characteristics and hydrodynamic system properties. We compare our 2D-models both to existing modeling studies in these regions and to own 1D-models ~~, which use climate station data, as it is common practice~~ that are conventionally based on climate
10 station input data. Our results show that our models are excellently suited to model karst spring discharge and rival the simulation results of existing approaches in the respective areas. The 2D-models show a better fit than the 1D-models in two of three cases, learn relevant parts of the input data themselves and by performing a spatial input sensitivity analysis we can further show their ~~potential for karst catchment localization and delineation~~ usefulness to localize the position of karst catchments.

Copyright statement. will be included by Copernicus

15 # 1 Introduction

Karst aquifers and karst springs are crucial for freshwater supply in many regions and 9% of the global population partly or fully rely on karst water resources (Stevanović, 2019). Karst systems in general are characterized by high heterogeneity due to the at least in large parts unknown conduit network, which controls the highly variable groundwater flow. This makes modeling difficult, hence a large variety of different approaches exists (Jeannin et al., 2021). Most of them require a certain level of back-

20 ground knowledge about the system in order to achieve high quality results. In contrary, deep learning approaches propose a convenient possibility of modeling by being able to establish a simple input-output relationship on their own, without detailed system knowledge necessary. Even though Artificial Neural Networks (ANN) are not a standard method in karst modeling yet, different types of ANNs have been applied in modeling karst water resources for quite a long time. In fact the study of Johannet et al. (1994), who showed that water infiltration modeling in karstic aquifers is possible with ANNs, was even one of the first ap-

25 plications of ANNs in water related research. The number of applications since then is increasing as for example documented by the reviews of Maier and Dandy (2000), Maier et al. (2010), and even more accelerating in recent years as shown by the reviews on applications in groundwater by Rajaee et al. (2019) and on hydrology and water resources in general by Sit et al. (2020). In this study, we apply 1D Convolutional Neural Networks (CNN) ~~, which have been shown to be fast and reliable for the closely related application~~ which were successfully applied in the related domains of groundwater level forecasting

30 ~~(Wunsch et al., 2021). We directly adapt this approach of using 1D-CNNs to the modeling of karst spring discharge time series. Although 1D-CNNs are frequently used to model time series in different contexts, besides some first rudimentary experiments (Jeannin et al., 2021),~~ (Wunsch et al., 2021; Afzaal et al., 2020; Lähivaara et al., 2019; Müller et al., 2020) and rainfall-runoff modeling (Van et al., 2020; Hussain et al., 2020). However, for spring discharge modeling they have not yet been applied~~to model karst spring discharge~~, besides some first rudimentary experiments in Jeannin et al. (2021).

35 Especially in direct comparison to concept based modeling, where shorter time series can be sufficient to achieve satisfying modeling results, one drawback of the 1D-CNN approach, as well as most other data-driven approaches, is the dependency on high data availability and quality. In many areas climate stations are often not available within the catchment of a spring, do not match the data availability of the discharge time series (period or temporal resolution), or are more distant and thus do not truly represent the events in the catchment itself. For this, gridded climate data can provide a solution, with reasonable time

40 periods and temporal resolutions being available from various products. Especially for karst springs it is difficult to simply extract corresponding time series from the gridded data, since this requires knowledge of the spring catchment and usually the available grid cells do not exactly match the catchment either. Besides the modeling purpose, the delineation of karst catchments is generally important to sustainably exploit but also protect karst water resources by establishing protection zones accordingly. Malard et al. (2015) explain that only few generalizable methods for karst spring catchment delineation have been proposed.

45 Instead, delineations usually rely on classical hydrogeological methods such as assessing geology, topography, hydrology, water balance, elaborate tracer tests and geophysical investigations. There has already been an attempt by Longenecker et al. (2017) to semi-automatically derive approximate catchment boundaries by correlating karst spring discharge events with global precipitation measurement (GPM) gridded data (NASA, 2016). The authors were able to achieve reasonable results with their method, but also noticed that they could not replace conventional methods.

50 Anderson and Radic (2021) have already applied gridded meteorological data to streamflow modeling in western Canada and used a ~~2D-CNN-LSTM model that is able~~ 2D-CNN in combination with a long short-term memory (LSTM) model to directly use ~~spatial~~ spatially distributed input data. LSTMs are recurrent neural networks, often used for time series modeling tasks. They showed that such models learn the relevant parts of the large scale gridded input data for each local or regional streamflow by themselves. We adapt and extent this approach to karst spring discharge modeling by establishing a ~~2D-1D-CNN model ,~~

55 ~~where the~~ similar model setup, however purely based on CNNs, where a 2D-CNN processes the spatially distributed input data and ~~the~~ a subsequent 1D-CNN performs the forecasting of the spring discharge time series ~~in accordance with the 1D-CNN approach based on climate station data. Thus,~~ . With this 2D-approach we can now directly use gridded meteorological data to potentially overcome the common data availability problems at climate stations, without the need for a prior description of the catchment area. ~~On the contrary~~Moreover, we investigate the potential of this approach for ~~catchment localization and delineation~~ identifying the approximate catchment location based on a modified spatial input sensitivity analysis ~~as performed in~~ from Anderson and Radic (2021). Deriving recharge areas based on rainfall-discharge event correlation, as previously done by Longenecker et al. (2017), requires (i) heterogeneous rainfall at catchment scale, (ii) precipitation data with sufficient spatial resolution that capture this heterogeneity and (iii) a karst system without too much dampening of the precipitation signals. This also applies to our proposed methodology, although we expect ANNs ~~to be superior at least for points (i) and (iii)~~being superior in representing non-linear relationships between rainfall and discharge.

In total, we explore the applicability of our proposed deep learning approaches with spatially distributed input data in modeling karst spring discharge in three different study areas. These study areas are well studied and for two of them several modeling publications, including also ANN approaches are available as benchmarks (Kong A Siou et al., 2011, 2012; Kong-A-Siou et al., 2013, 2014). We further compare the results with own 1D-CNN models using conventional climate station input data. As spatially distributed inputs we use either hourly ERA5-Land reanalysis data (Muñoz Sabater, 2019) or daily E-OBS data (Cornes et al., 2018), depending on the temporal resolution of spring discharge data. Finally, we explore the potential of the 2D-approach for karst spring catchment localization ~~and delineation~~ by investigating the spatial input sensitivity of the trained CNN models.

2 Data and Study Areas

2.1 Overview

In this study, we investigate three different karst springs: Aubach spring in the Hochifen-Gottesacker area in Austria (Fig. 1a), springs of Unica river in Slovenia (Fig. 1b) and Lez spring in southern France (Fig. 1c). All springs show different characteristics regarding relevant system properties (e.g. catchment size, complexity of the hydrological system), environmental conditions (e.g. dominant climate, anthropogenic forcing) and data availability (see also Table A1). Furthermore, all areas are well studied, existing data was easily accessible and except Unica, several previous modeling approaches are available for comparison.

2.2 Aubach Spring, Austria

Aubach spring is a major karst spring in the Hochifen-Gottesacker karst area in the northern Alps at the border between Germany and Austria. Southern border of the area is the Schwarzwasser valley, which geologically forms the contact zone between the Helvetic Säntis nappe in the north and sedimentary rocks of the Flysch zone in the south (Goldscheider, 2005). In the northern part the dominant karst formation is the Schrattenkalk formation, a cretaceous limestone with a thickness of about
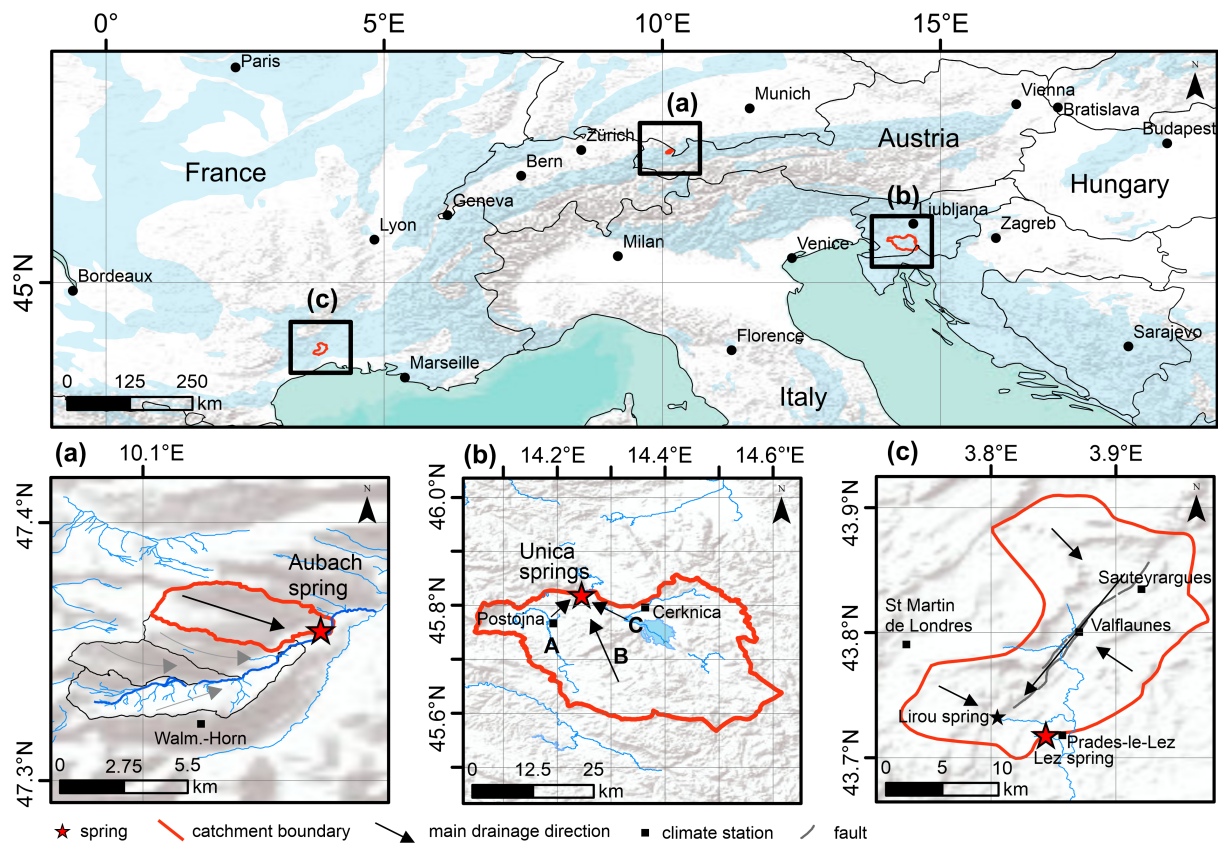
3

Figure 1. Overview of all three study areas, the simulated springs (red star) and their catchments (red lines). Black squares indicate locations of climate stations used for 1D-modeling (not all are shown in these maps), blue shadings in the upper map show karst areas based on WOKAM (Chen et al., 2017a) (a) Hochifen-Gottesacker karst area and Aubach spring, black lines depict minor contributing sub-catchments; (b) Unica river springs and Javorniki karst plateau (B); (c) Lez spring catchment, Lirou overflow spring (black star) and major fault Corconne-Les Matelles (grey line);

100 m. This Schrattenkalk is structured in folds, which hydrogeologically form parallel sub-catchments (Fig. 1a) that contribute to different proportions to the several springs in the valley (Goldscheider, 2005; Chen and Goldscheider, 2014). In this study we focus on one large, non-permanent spring called Aubach spring (1080 m asl, discharge up to 10 m^3/s). The Hochifen-Gottesacker area is largely influenced by seasonal snow accumulation and melting in the elevated regions (>1,600 m asl),

90   which is also clearly reflected in the discharge of Aubach spring by increased baseflow and daily snowmelt-induced variations, especially in the months of April to June. Earlier studies by Goldscheider (2005) and Chen and Goldscheider (2014) have identified one major catchment area of Aubach spring with approximately 9 km^2 (Fig. 1a), still, to smaller parts upstream catchments can also contribute to Aubach spring discharge. This applies also to the non-karstified Flysch area directly in the South (southernmost sub-catchment in Fig. 1a), where precipitation events are only relevant during low flow conditions.

95   Then, the surface runoff from this area sinks into an upstream estavelle and contributes via an underground connection to the

discharge of Aubach spring. During high flow conditions, the estavelle itself acts as an overflow spring and no contribution from surface runoff at Aubach spring occurs. Generally, the climate in the area can be described as cooltemperate and humid and the mean annual precipitation at the closest used climate station in this study (Walmendinger Horn) is about 2000 mm (2003-2019).

100   For this study Aubach spring is selected because of the good data availability. We use 8 years of hourly discharge data provided by the office of the federal state of Vorarlberg, division of water management, and we further use precipitation and temperature data from three surrounding climate stations: Oberstdorf, Walmendinger Horn (shown in Fig. 1a) and Diedamskopf. Additionally, due to the high importance of snow in the area, we run a snowmelt routine as preprocessing of the meteorological input data as described in Chen et al. (2018). This routine is a slightly modified version (after Hock, 1999) of the HBV hydro-

105   logical model snow routine (e.g. Bergström, 1975, 1995; Kollat et al., 2012; Seibert, 2000), which redistributes the precipitation time series in accordance with probable snow accumulation and snowmelt.

2.3   Unica Springs, Slovenia

The Unica springs (450 m asl) are located on the southern edge of a karst polje in SW Slovenia and are important from a biodiversity and water supply perspective. There are two permanent and several temporary springs that feed the Unica river.

110   The joint discharge during 1989-2018 ranged from 1 to 90 m^3/s, while the mean discharge was 21 m^3/s (ARSO, 2020a). The springs are fed by three clearly distinguishable sub-catchments covering an area of about 820 km^2. The main recharge area is the highly karstified Javorniki plateau (up to 1,800 m; marked B on Fig. 1b), whose predominant lithology is Cretaceous rocks, mainly limestones, changing in places to dolomites and breccias. To a lesser extent, Jurassic and Palaeogene carbonate rocks are also present. The thickness of the unsaturated zone is estimated to be up to several hundred meters (Petrič et al., 2018,

115   and references therein). To the east, the hydrology of the area is controlled by a strike-slip fault zone, along which a chain of karst poljes developed (between 500 and 700 m; marked C on Fig. 1b). Upper Triassic dolomites predominate, changing to Jurassic limestones and dolomites in the south and west, forming aquifers with fracture porosity, which in places have very low to moderate permeability, and in some parts a superficial river network forms. As the karst poljes follow each other in a downward series, they are connected in a common hydrological system with transitions between surface and groundwater flows

120   and frequent flooding (Mayaud et al., 2019). In the west, the Pivka River Basin (between 500 and 700 m; marked A on Fig.1b) consists of poorly permeable Eocene flysch in the north, which conditions a surface river network. The southern part consists of Cretaceous and Jurassic carbonate rocks forming a shallow karst aquifer. Surface flow occur during high water levels, receiving additional water from intermittent springs on the western foothills of the Javorniki. The water flow of the sinking rivers in the subsurface from the A and C parts is clearly of the channel flow type. The springs were selected for this study

125   because they drain a complex binary karst system of the so-called Classical Karst, they are well studied with a large amount of hydro-meteorological data and their hydrology is influenced by ~~significant~~ substantial snow accumulation and melting. The catchment belongs to the moderate continental climate and is mostly covered with forests. For this study we use daily discharge data from the Unica-Hasberg gauging station (in the following called Unica) (ARSO, 2020a) and daily meteorological data from Postojna and Cerknica meteorological stations ranging from 1981 to 2018 (ARSO, 2020b). The meteorological stations

130 (squares in Fig. 1b) are located on the western (Postojna) and eastern (Cerknica) part of the catchment, representing different climate regimes and are separated by the karst massif in between. For Postojna station the following parameters are available: precipitation (P), temperature (T), potential evapotranspiration (PET), relative humidity (rH), snow (S) and new snow (nS). For Cerknica station only P, S and nS are available. Average annual precipitation during 1989-2018 is about 1500 mm and on average, there are 33 days of snow cover per year in Postojna (530 m), while even longer snow cover is expected on the plateau.

135 ## 2.4 Lez Spring, France

Our third study area is located 15 km north of Montpellier in France, within a large and complex karst system delimited by rivers and marly terrains. Eastern and western borders are the Vidourle and Hérault river valleys, northern and southern borders are piezometric limits. At larger scale northern and southern boundaries are structural boundaries due to Cévennes and Montpellier faults, respectively. The dominant karst formations are Argovian to Kimmeridgian, and Berriasian massive
140 limestones with 650 m to 1000 m thickness. Infiltration occurs mostly diffuse but also localized through fractures and sinkholes along the basin and through the major geologic fault of Corconne-Les Matelles in the northern part of the basin (indicated by a grey line in Fig. 1c).

The hydrogeological basin associated to the Lez spring has been estimated to be about 240 km^2 (Fig. 1c) on the basis of the hydrodynamic response to high discharge continuous pumping into the saturated zone of the aquifer (Thiéry and Bérard, 1983).
145 However, the effective recharge catchment of the Lez spring, which corresponds to the extent of Jurassic limestone outcrops, has been estimated to be about 130 km^2 (Fleury et al., 2009; Jourde et al., 2014). The Lez karst aquifer is under anthropogenic pressure (i.e. aquifer exploitation for water supply) with pumping performed directly within the karst conduit. The discharge is measured at the spring pool and is regularly null during low water periods, when the pumping rate exceeds the natural spring discharge. Ecological water discharge towards the Lez river (160 L/s then 230 L/s after 2018) is ensured during such periods by
150 a partial deviation of the pumped water to the river. Lirou spring (Fig. 1c) is the main of several overflow springs that activate during high flow periods (Jourde et al., 2014).

The Lez catchment is exposed to a Mediterranean climate, which is characterized by hot and dry summers, mild winters and wet autumns. Analyses by MeteoFrance show that on average 40% of the annual precipitation occurs between September and November with a high variability across years (Bicalho et al., 2012). The average annual rainfall rate for the 2008-2018 period
155 is 904 mm.

For this study, the modeling is based on nearly 10 years of daily discharge data provided by SNO KARST (Jourde et al., 2018; SNO KARST, 2021). The temperature data is from the Prades-le-Lez climate station; we use, however, an interpolated precipitation data series that is derived from a weighted average of four rainfall stations (Fig. 1c) (similar to Fleury et al., 2009; Mazzilli et al., 2011), three of them being located on the Lez catchment (Prades-le-Lez, Valflaunès, Sauteyrargues). The
160 fourth station (Saint-Martin-de-Londres) is located few kilometers west of the catchment. Interpolation is in principle possible in this area due to the existing topography; at the same time, interpolation based on Thiessen-polygons (compare Appendix B) also allows compensation for data gaps at single stations. We decided to apply this preprocessing, because all but Saint-Martin-de-Londres climate station show such gaps from time to time, which explains the benefit from including within-catchment

precipitation. Including pumping data is not favorable in this study, because these were only available for a shorter period of time and such data would also not be available for a real forecast in the future (in contrary to weather and climate data).

For Lez spring, results from several existing modeling approaches, including several ANN studies, are available. Please refer to Kong A Siou et al. (2011) for an overview about older modeling studies at Lez spring with different approaches. Here, we focus on the most recent studies for comparison, all of which were conducted with ANNs (Kong A Siou et al., 2011, 2012; Kong-A-Siou et . These studies are based on modeling Lez spring using Multi-Layer-Perceptrons (MLP) or recurrent MLPs. They use a wide variation of daily data from different time periods and also have different study goals. Darras et al. (2015, 2017) focus only on single events to evaluate flash flood forecasting, while Kong-A-Siou et al. (2013, 2014) and Kong-A-Siou et al. (2015) can be best compared to the work presented here.

2.5   Spatial Climate Data

Besides climate station data, we explored raster data from the E-OBS (Cornes et al., 2018), the ERA5-Land (Muñoz Sabater, 2019) and from the RADOLAN (DWD Climate Data Center (CDC)) as spatially distributed model inputs. E-OBS provides daily gridded meteorological data for Europe from 1950 to present, derived from in-situ observations, ERA5-Land provides hourly reanalysis data from 1981 to present. Both are available with a spatial resolution of $0.1° \times 0.1°$ (approx. 8 km x 11 km for all study areas). Depending on the dataset, different sets of parameters are available. In case of E-OBS we initially provide our models with precipitation (P), mean, minimum and maximum temperature (T, Tmin, Tmax), relative humidity (rH) and surface shortwave downwelling radiation (Rad). For ERA5-Land, where a ~~significantly~~ substantially larger set of parameters is available, the following were used as initial inputs: total precipitation (P), 2m temperature (T), total evaporation (E), snowmelt (SMLT), snowfall (SF) and volumetric soil water of all four available layers (SWVL1: 0 - 7 cm, SWVL2: 7 - 28 cm, SWVL3: 28 - 100 cm, SWVL4: 100 - 289 cm). Relevant input parameters from both datasets are later selected through Bayesian optimization (see section 3.3). The spatial extent of the input data is chosen very generously for each spring, so that between 6 and 8 additional cells are available as input data around the respective catchments. This prevents a predefinition of the area that needs to be identified as relevant as well as reduces the influence of possible border effects due to the CNN approach using 3x3 filters (compare methodology section). The resolution of ERA5-Land and E-OBS data corresponds to the grid cell size shown in the catchment plots in Figures 1a-c, although each showing a slightly different absolute position of grid center points. We already see that the relation of grid resolution to catchment size varies strongly, with Aubach catchment being the smallest and Unica catchment being the largest. Depending on the temporal resolution of the available spring discharge measurements, we choose the spatial input data in accordance, thus E-OBS for Unica and Lez spring, ERA5-Land for Aubach spring.

Compared to the catchment size of Aubach spring (about $9 \, \text{km}^2$), the spatial resolution (approx. 8 km x 11 km) of the gridded input data is extremely coarse. We therefore additionally explore a combination of ERA5-Land input parameters (except P) with radar based precipitation data (RADOLAN) that offers a spatial resolution of 1 km x 1 km (DWD Climate Data Center (CDC)). For each of the RADOLAN grid cells, the according parameter value of the ERA5-Land data is chosen, where the RADOLAN grid cell center lies in. This corresponds to the simplest form of downscaling. For this analysis, we reduce the

7

spatial extent of the 2D-input data to save calculation time, but increase the number of cells compared to the ERA5 section around Aubach spring due to the higher resolution of the RADOLAN grid.

3 Methodology

3.1 Modeling Approach

In this study, we simulate karst spring discharge with deep learning models using meteorological input data. As proof of feasibility, we use meteorological data from surrounding climate stations. However, these stations often show limited data availability in terms of the number of parameters (mostly limited to precipitation and temperature, rarely more), the record length, as well as the sampling interval. Also, the spatial coverage and proximity is often unsatisfactory, which especially in mountainous regions can introduce a distinct error of parameters with high spatial variability such as precipitation.

Gridded meteorological data can offer a solution to these issues, as they usually provide good temporal coverage and resolution, a reasonable spatial resolution as well as a large-scale (e.g. continental or even global) availability. Further, especially reanalysis data include a larger parameter set. However, when the catchment of the spring is unknown, it remains unclear which cells to retrieve time series from when using 1D-time series as inputs. Based on our revised version of the approach of Anderson and Radic (2021), we demonstrate a solution by processing 2D-inputs and letting the model decide by itself, which parts of the input data are relevant to model the spring discharge.

3.2 Convolutional Neural Networks (CNN)

Convolutional Neural Networks (LeCun et al., 2015) are widely applied in several domains such as object recognition, image classification, and signal processing. The structure of most CNN models is based on the repetition of blocks that are made up of several layers, typically at least one convolutional layer followed by a pooling layer. The former matches the dimension of the input data (e.g. 2D for image alike data, 1D for sequences such as time series) and uses filters with a fixed size (receptive field) to produce feature maps of the input. The latter performs down-sampling of the produced feature maps and hence increases the density of information. A large variety of model structures based on such blocks, in combination with additional layers in between to prevent exploding gradients (e.g. batch normalization layers (Ioffe and Szegedy, 2015)) or model overfitting (e.g. dropout layers (Srivastava et al., 2014)) are possible; however CNNs usually end with one or several fully connected dense layers to produce a meaningful output.

~~In this study, we use 1D-CNN models as we have shown earlier that these~~ From our experience in preliminary work and earlier studies (Wunsch et al., 2021; Jeannin et al., 2021) we know that 1D-CNNs are fast, reliable and excellently suited for modeling hydrogeological time series~~(Wunsch et al., 2021). Especially~~, such as groundwater levels or spring discharge. We have shown that they are faster compared to LSTMs, which are often the method of choice ~~, they are more stable and significantly faster, while showing similar performancefor this specific application. We adapt this approach and~~ for time series modeling, and even outperform them or at least show similar performance. This is in agreement with the findings of
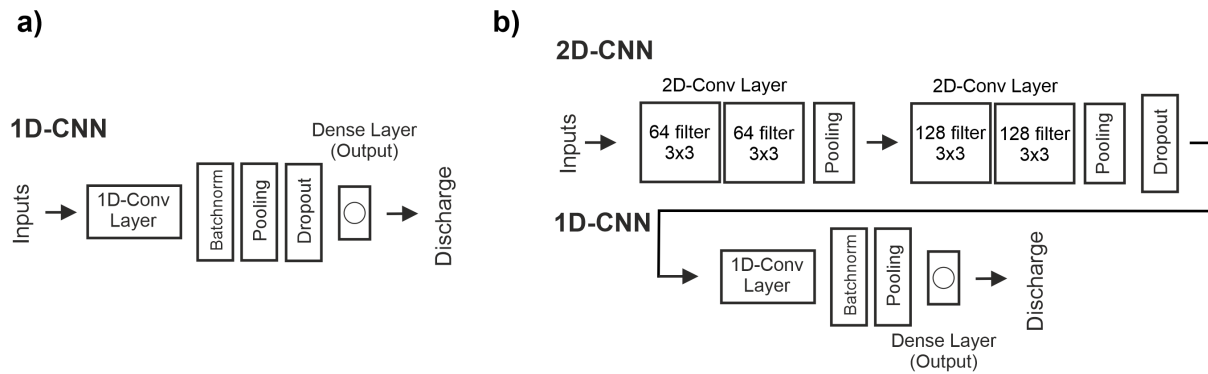
8

Figure 2. Model structures applied for modeling karst spring discharge based on climate station data (a) and gridded meteorological input data (b). Flatten layers are not displayed.

(Van et al., 2020) in the domain of rainfall-runoff modeling. We therefore perform karst spring discharge modeling in two different setups. One setup uses 1D-meteorological input data from surrounding climate stations, the other one uses gridded

230 climate data as input and thus combines the 1D-CNN model with a time distributed 2D-CNN model~~to process the 2D-input data.~~. The 2D-CNN model processes the spatially distributed input data, while the 1D-CNN is used for time series forecasting in both setups. Using a 1D-CNN subsequent to the 2D model instead of a LSTM, as in Anderson and Radic (2021) for example, makes both setups methodologically consistent and improves the comparability among them. The general model structure of both setups is shown in Figure 2. They basically use the same 1D-model except the position of the dropout layer. We use

235 Bayesian hyperparameter optimization to select the 1D-filter number, batch-size and input sequence length of each model in both setups.

To reduce the dependency on the random initialization of the models, we use an ensemble with 10 members, each based on a different pseudo-random seed. Further, we implement Monte-Carlo dropout to estimate the model uncertainty from a distribution of 100 results for each ~~calculation of each model performed~~ of the ten realizations of each model in this study. ~~Our~~

240 We derived the 95% confidence interval from these 100 realizations by using 1.96 times the standard deviation of the resulting distribution for each time step. Each uncertainty was propagated while calculating the overall ensemble mean value for final evaluation in the test set. This uncertainty is shown as confidence interval for each of our simulation results in the following. We want to point out, that this uncertainty does not include other sources (such as input data uncertainty) but the random number dependency. All our models are implemented in Python 3.8 (van Rossum, 1995) and we use the following libraries

245 and frameworks: Numpy (van der Walt et al., 2011), Pandas (McKinney, 2010; Reback et al., 2020), Scikit-Learn (Pedregosa et al., 2011), Unumpy (Lebigot, 2010), Matplotlib (Hunter, 2007), BayesOpt (Nogueira, 2014), TensorFlow and its Keras API (Abadi et al., 2015; Chollet, 2015).

9

3.3 Model Calibration and Evaluation

We split the time series data for each site into four parts according to Table 1. While the first part is used for training, the second part (validation) is simultaneously used to prevent the model from overfitting via early stopping. The model's hyperparameters are optimized according to its performance on the optimization set, while the last set is used as completely independent test set for final evaluation of the model performance without data leakage from training or optimization. Training epoch number

Table 1. ~~Time series~~ Data splitting schemes for all study areas (number of values in parentheses).

	Time Interval	Training	Validation	Optimization	Testing
Aubach spring	Hourly	2012-2017	2018	2019	2020
		(44,807)	(8,760)	(8,760)	(7,320)
Unica spring	Daily	1981-2012	2013+2014	2015+2016	2017+2018
		(11,687)	(730)	(731)	(730)
Lez spring	Daily	2008-2016	2017	2018	2019
		(2,629)	(366)	(365)	(701)

and early stopping patience are varied manually for each model at each test site. Hyperparameters for the 1D-CNNs of both setups are optimized on the respective optimization set as stated above, maximizing the sum of Nash-Sutcliffe efficiency and R^2 (calculated as explained below). The number of optimization steps is also varied manually for each model and is always a trade-off between accuracy and computational costs. In case of many available input parameters we treat input parameter selection equally as a global optimization problem and use Bayesian optimization to simultaneously select a proper set of input parameters and hyperparameters. Thus, input optimization is used for each 2D-model, as ERA5-Land and E-OBS offer several different meteorological parameters, as well as to the 1D-model of Unica springs. For Lez spring and Aubach spring, only a smaller input parameter set is available and hence fully used. For all models we offer an additional input (Tsin), which is a sinus curve fitted to the temperature data. This parameter can provide the model with information on seasonality and on the current position in the annual cycle (Kong-A-Siou et al., 2014). Precipitation is the only parameter that is not optimized but fixed as input, because it has undoubtedly the most important influence on the discharge of a karst spring. The optimized hyperparameters, information on some fixed hyperparameters, and a summary of the number of parameters in each model, is given in Appendix Table D1.

We calculate several metrics to evaluate the performance of our models: Nash-Sutcliffe Efficiency (NSE) (Nash and Sutcliffe, 1970), squared Pearson r (R^2), root mean squared error (RMSE), Bias (Bias) as well as Kling-Gupta-Efficiency (KGE) (Gupta et al., 2009). For squared Pearson r we use the notation of the coefficient of determination (R^2), because we compare the linear fit between simulated and observed discharge, thus of a simple linear model, which makes them equal in this case.

3.4 Spatial Input Sensitivity and Catchment ~~Delineation~~Localization

Anderson and Radic (2021) show in their study that when using 2D-input data for CNNs for streamflow modeling, there is physical meaning in the way that spatial fractions of the input data are learned to be more important than others. We modify this approach and transfer it to karst spring modeling, where we demonstrate that this approach ~~has even some potential for karst spring catchment delineation, which to date is dependent on elaborate tracer tests~~to qualitatively localize karst catchment locations.

We use the Gaussian spatial perturbation approach from Anderson and Radic (2021)~~and modify it~~, which is similar to other input sensitivity algorithms such as occlusion (Zeiler and Fergus, 2014) or RISE (Petsiuk et al., 2018), but in contrary to these methods takes into account the physical meaning of the absolute parameter value for each pixel during the perturbation. We modify this approach so that only a single channel (input parameter, e.g. precipitation) is perturbed at a time for the sensitivity analysis. For details of this approach we refer to the original study. In short it works by perturbing spatial fractions of the input data by ~~using~~ adding or subtracting a 2D-Gaussian curve from the input data at a certain location. The perturbed data is passed through the trained model to determine the resulting error from the specific perturbation. In this way, after many repetitions, heat maps are created that show how sensitive the trained model is to perturbations of certain areas of the input data. In the case of karst spring modeling we perturb only single channels, instead of all channels at once as in the original approach, for the following reasons. We use some very different input parameters and ideally want to separate the individual influence of each of these channels. Also these parameters show a very different spatial heterogeneity and variability (i.e. spatial autocorrelation), which means that the model can learn the importance for example of temperature from a large area, as long as it favors a lower simulation error, while for precipitation ideally a smaller area ~~will most certainly~~ corresponding to the catchment should have a higher influence on the spring discharge and therefore has to be learned more accurately. ~~Furthermore we mainly focus on the precipitation channel~~ The intended use for catchment localization~~and delineation, because on the one hand we have a high spatial variability and on the other hand it is undoubtedly the major parameter that defines the catchment in karst areas~~, which especially in Karst areas is driven by precipitation predominantly, makes it necessary to separate the influence of each channel.

4 Results and Discussion

4.1 Aubach Spring

Figure 3a shows the simulation results of the 1D-CNN model for the test period 2020, using only available climate station data. Error measures indicate a high accuracy of the model simulation, NSE and R^2 values both are 0.74, KGE is 0.79. ~~Overall, this is a satisfying fit of a complex time series.~~ We observe that peaks in winter and spring are underestimated but the snowmelt period, clearly visible by increased baseflow and daily variations from April to June, is nicely fitted, as well as the following summer peaks. A short series of discharge peaks in the end of September/beginning of October is not captured. We assume that these were caused by small-scale precipitation events that are not represented in the data of the climate stations used as inputs. Interestingly, daily variations, which ~~are probably~~ might be learned during the snowmelt period, are also visible in periods not

11

influenced by snow (e.g. in August). From experience (Chen et al., 2017b) we know the high relevance of snow in this area and by coupling the CNN model with a snow routine data preprocessing, we are able to further improve the model performance (Fig. 3b). We now can achieve a fit with 0.77 for both NSE and R^2, KGE increases to 0.84. Our model is able to nicely fit the

305 second largest peak of the whole dataset, which occurs in February, though, the peak is slightly overestimated, whereas other peaks still tend to be underestimated. The snowmelt period remains well simulated, but shows increasing deviations close the end of the period. The earlier noticed daily variations in summer and autumn, now no longer appear, which is most certainly an effect of the snowmelt preprocessing.

Please note that the 95% model uncertainty from random number dependency, estimated from 10 ~~different~~ differently

310 initialized models with a Monte-Carlo dropout distribution from 100 runs each (i.e. 1000 simulations in total), is very low for both modeling results (a+b) compared to the overall variability of the discharge. ~~Major source of uncertainty is therefore probably the especially~~ In general, we assume the spatially limited input data to be the major source of uncertainty, as all climate stations have a certain distance to the catchment area; however, as explained in the methods section, such uncertainty is not included in the confidence interval shown in the plots. Other modeling approaches (Chen and Goldscheider, 2014; Chen et al.,

315 2017b, 2018) based on three successive and improved versions of a combined lumped parameter (SWMM) and distributed model achieve similar or higher NSE values for the simulation of Aubach spring discharge (0.92, 0.83, 0.80 respectively) but in contrary to our approach simulate three springs simultaneously. However, these results are hardly comparable with each other and neither with this study. Reasons are (i) different data basis regarding the number and position of climate stations used as input data, (ii) different simulation periods as well as (iii) very different test set lengths. The shortest test set only had 40

320 days (in autumn), the longest (Chen et al., 2017b) used one year of data for model calibration and performed a split-sample test on the same data set. Despite our model shows a slightly lower NSE value compared to these three models, it is in the same ~~order of magnitude and performs probably~~ range and we assume it to perform at least equally as none of the previous studies covered a complete annual cycle as contiguous test period, including high peaks in late winter and strong snowmelt influence in spring and early summer.

325 Figure 3c shows the results of the 2D-modeling setup using (only) ERA5-land input data. Based on Bayesian optimization, besides the fixed and not optimized input P, the following input parameters are selected: T, E, SMLT, SWVL2 and SWVL4 (for a comparison of selected parameters with other study areas see also Table A1). The performance of the 2D-model is similar to that of the 1D-models, showing a NSE (0.76) and RMSE in-between both, a larger R^2 (0.8) but a lower KGE (0.71). This performance is still ~~very satisfying~~ high considering that the major catchment is extremely small (about $9\,km^2$) compared to

330 one ERA5-Land grid cell, and that a large grid section of 14 x 14 ERA5-Land cells (1.4° x 1.4°) was used as input. We see that the major peak in February is slightly underestimated, as well as the beginning of the snowmelt period in April; however, the end of this period in May/June has improved now compared to (b). Both 1D-models are superior in estimating the peaks especially during summer, except the already mentioned peaks in September/October, which have improved using the 2D-input data. This supports the assumption that the climate stations do not represent these precipitation events, but the 2D-data does.

335 To account for the small area of the catchment of Aubach spring, Figure 3d shows the results of the 2D-input data, using the spatially higher resolved RADOLAN precipitation data in combination with downscaled ERA5-Land data for all other param-
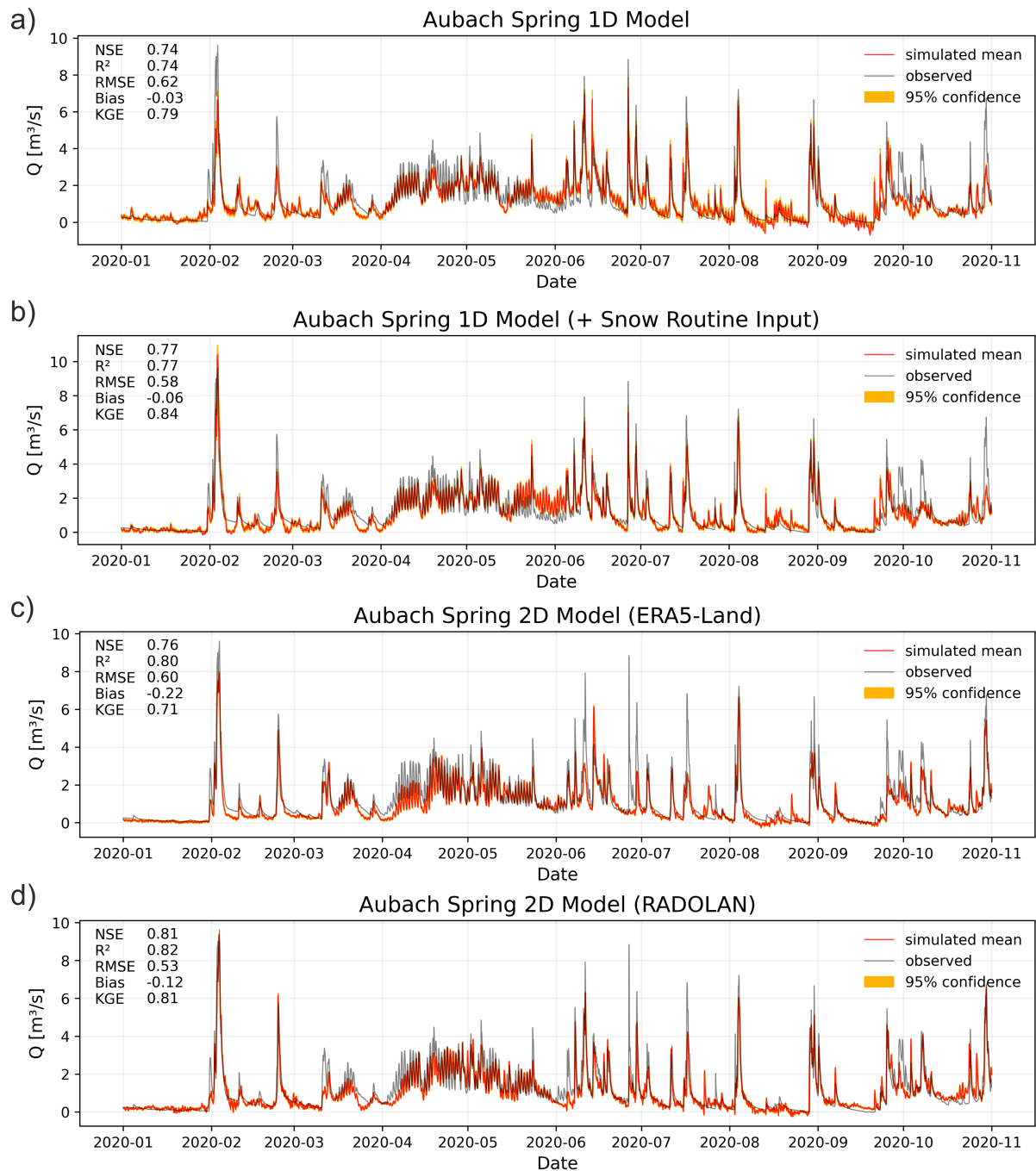
Figure 3. Simulation results for the year 2020 at Aubach spring: (a) 1D-model based on climate station inputs, (b) 1D-model with additional snow routine preprocessing, (c) 2D-model based on ERA5-Land gridded data and (d) 2D-model with combination of ERA5-Land data and RADOLAN precipitation input.

eters. We have reduced the spatial extent of the 2D-input, but use an even higher grid cell number (22 x 22 or 22^2 km^2), with a reasonable buffer around the catchments. Additionally to P, the optimized model uses inputs from all available parameters except E and SWVL3, thus T, Tsin, SMLT, SF, SWVL1/2/4. This model shows the best performance of all four models by reaching ~~an~~ a NSE of 0.81, R^2 of 0.82 and KGE of 0.81. Similar to the model in (c), the beginning of the snowmelt period in April remains slightly underestimated and compared to the 1D models ~~and~~ the peaks in summer are less well fitted. Nevertheless, we generally see ~~a very satisfying fitof the simulation results~~an accurate fit, especially the largest peak in February is ~~simulated almost perfectly~~well represented. Compared to the 1D-approach, the main source of uncertainty for both 2D-models ~~is probably~~ should be the uncertainty of parameter values resulting from the ERA5-land grid cell sizes, which is too large compared to the catchment size. Improved downscaling of ERA5 data or other high resolved climate data for a combination with RADOLAN precipitation data might be a promising approach for simulating small catchments like this one. Model uncertainty derived from random number effects and Monte Carlo dropout is (equally to the 1D-models) satisfyingly small. In total we see that both the 1D and the 2D approach for this catchment bear ~~significant~~ substantial uncertainties in terms of input data, even though the results are ~~quite satisfactory~~generally very accurate. On the one hand the climate stations represent the true observed climate, on the other hand this is true only for a very specific point, in this case even outside the catchment and embedded into a highly variable topography. The 2D data, however, shows too large grid cell sizes for Aubach spring catchment and is itself modeled (in case of ERA5-Land). We therefore do not think that one approach is superior in terms of uncertainty for this study area, but we can show that even in this case with relatively course gridded input data compared to the catchment size, the 2D-approach offers a decent alternative.

4.2 Unica Springs

Figure 4 summarizes the 1D- and 2D-model performance on the years 2017 and 2018 for Unica springs in Slovenia. ~~Due to highly complex hydraulic behavior in this study area, which is for example related to large polje floodings and to a strongly variable water level in the system that varies also the catchment area, extracting the highly non-linear precipitation-discharge is especially challenging in this study area. We generally observe less dynamics in terms of the number of flood pulse events compared to Aubach spring. But in terms of intensity of hydrologic variability, discharge rates can vary by many orders of magnitude. This is primarily due to the large size of the catchment area, the very high degree of karstification of the carbonate rocks, and the fact that the main spring may acts as an overflow spring. Many high flow events have a quite long duration of days to even weeks resulting in a plateau-like shape. This is due to the regular flooding of the polje. After the drainage areas of the polje are completely flooded, there is a progressive back-flooding and a steady rise in the water level, which makes it impossible to accurately monitor the inflow conditions.~~ The simulation of this quite large catchment area (820 km^2) is based on the data of only two climate stations (Postojna and Cerknica). All available input parameters from both stations except relative humidity from Postojna station and new snow from Cerknica station were used as inputs as selected by the Bayesian optimization model. The 1D-model shows solid performance overall (NSE: 0.73, R^2: 0.79, KGE: 0.63), including reaction for all major discharge events. ~~Recessions~~ However, recessions especially in 2017 are estimated ~~significantly~~ substantially too conservative and the plateau shapes of the large peaks (e.g. January 2018) are not well captured, but rather simulated as multiple peaks. ~~Conceptually~~

~~this might be~~ In general, many high flow events have a quite long duration of days to even weeks resulting in such plateau-like shapes. This is due to the regular flooding of the polje. After the drainage areas of the polje are completely flooded, there is a progressive back-flooding and a steady rise in the water level, which makes it impossible to accurately monitor the inflow conditions. Therefore, simulating multiple peaks might be conceptually even more true than the plateau-like shape, however not easy to evaluate. The peak in April 2018 is quite clearly underestimated, whereas the following low flow period (summer 2018) is slightly overestimated. One possible reason could be ~~significant~~ substantial environmental changes that occurred in the catchment during 2014-18 (Kovačič et al., 2020). During this period a considerable amount of vegetation was destroyed by a series of large-scale forest disturbances. We expect the evapotranspiration changed due to changes in canopy interception, water use, and soil moisture. As a result, spring behavior has likely changed, because vegetation cover is an important element of the water balance and recharge events may have resulted in higher infiltration rates and more intense spring response, as well as more pronounced droughts. Because the period prior to 2014 was part of the training data (1981-2012), the change in spring behavior could not be predicted, resulting in an observed modeling incompatibility.

Due to highly complex hydraulic behavior in this study area, which is for example related to large polje floodings and to a strongly variable water level in the system that varies also the catchment area, extracting the highly non-linear precipitation-discharge is especially challenging. We generally observe less dynamics in terms of the number of flood pulse events compared to Aubach spring. In terms of intensity of hydrologic variability, discharge rates can vary by many orders of magnitude. This is primarily due to the large size of the catchment area, the very high degree of karstification of the carbonate rocks, and the fact that the main spring may acts as an overflow spring.

~~Using~~ By using the 2D-input data from 18 x 21 E-OBS grid cells we were able to improve the model performance ~~significantly~~ substantially (Fig. 4b), showing now a NSE of 0.83, R^2 of 0.84 and KGE of 0.80. Selected input parameters are: P (fixed), Tmax, rH and Rad. We generally observe a similar shape of the simulation as for the 1D-model but with overall reduced errors. Still, the plateau shape of some peaks is not well captured but the same conceptual understanding as for the 1D-model seems to be learned. Recessions are generally too conservative, especially the simulation of low flow periods and minor discharge events improve clearly though. These results are plausible, as minor discharge peaks are ~~probably~~ presumably due to small precipitation events, which ~~are probably not~~ may not be reflected in the selected climate station data, but visible in the gridded data derived from a larger set of observational points. ~~We have, however, noticed that training the 1D-model with data starting 1961 (20 years earlier), can still significantly improve the performance, similar to the 2D results shown here. We do not provide these results as they were produced in a slightly different model setting, not fully consistent with this work. To fully exploit the gridded parameter set and maintain comparability, the results shown here are based on a start in 1981, which corresponds to the start date of rH from the E-OBS data (other parameters start earlier).~~ As for Aubach spring, both models show a comparably low uncertainty based on random number variation and Monte-Carlo dropout, the uncertainty of the 2D-simulation is even a bit lower than for the 1D-model. ~~The~~ Again, we assume the spatially limited climate station data to be the main source of uncertainty in the 1D-model~~is probably the spatially limited climate station data~~, because meteorological stations are located on the western and eastern side of the karst massive. The karst massive itself represents the orographic barrier with different temperature and precipitation regimes that are certainly not captured by the considered meteorological stations. For 2D-data,
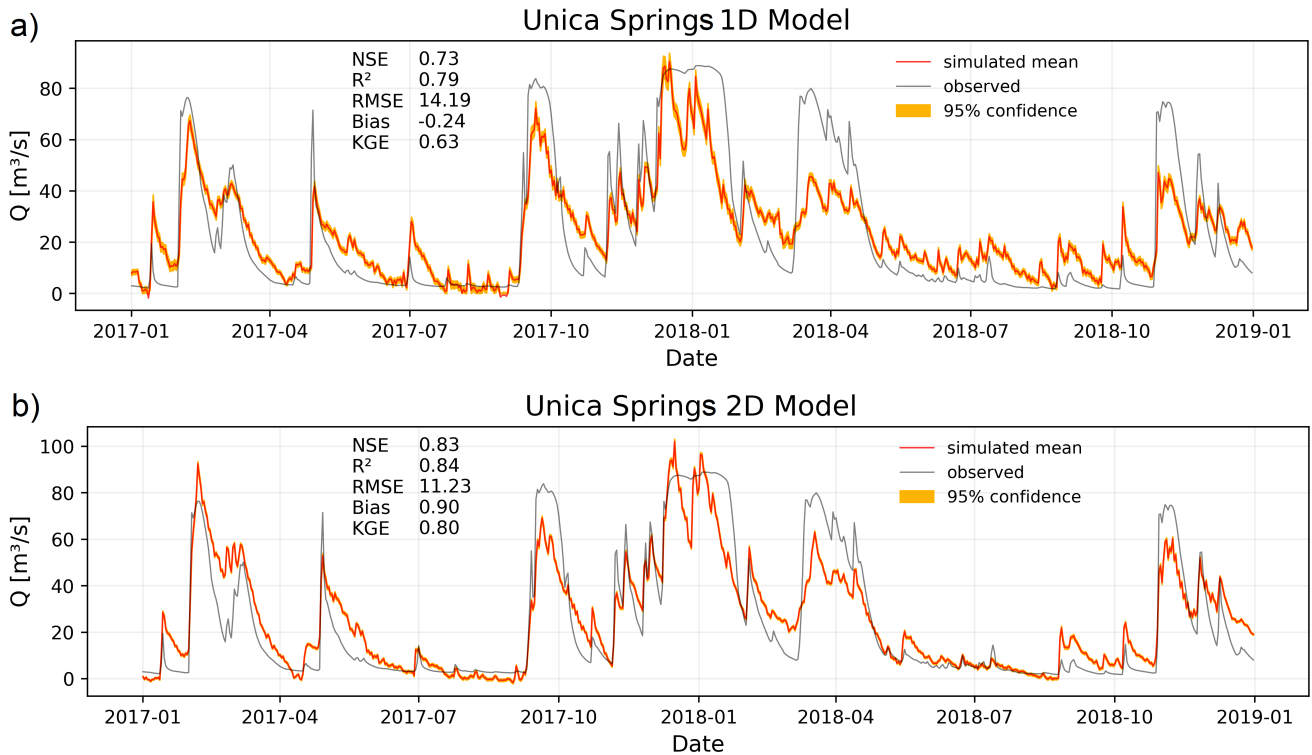
Figure 4. Simulation results for 2017-2018 at Unica springs in Slovenia using climate station input data (a) and E-OBS gridded data (b).

the general grid uncertainty may be comparably low ~~,~~ due to the large size of the catchment. Several earlier modeling studies were conducted in the area of the Unica catchment (e.g. Kaufmann et al., 2016; Mayaud et al., 2019; Kaufman et al., 2020; Kovačič et al., 2020) even including ANNs (Sezen et al., 2019), but none of these directly modeled Unica springs discharge, but rather focused on other aspects like cave hydraulics or polje modeling.

4.3 Lez Spring

Lez spring represents a third class of study area, as the catchment size (around $240\,\mathrm{km}^2$) is somewhere in between the two others, the climate is Mediterranean and the spring runs dry for a ~~significant~~ considerable amount of time during the annual cycle due to a constant exploitation of the karst aquifer through pumping. Figure 5 shows both the results for the 1D- (a) and the 2D-model (b). Despite comparably short training (daily data, starting in 2008) we observe a very high fit of the 1D-model above 0.86 for NSE, R^2 and KGE. As well the timing of the peaks, the absolute height of the peaks, as the dry periods are simulated ~~very well~~accurately, except some deviations in early 2019.

For the 2D-model we use input from 19 x 18 E-OBS grid cells and the Bayesian model selects only rH and Rad as inputs besides the fixed input P. Considering the high relevance of potential evapotranspiration in Mediterranean areas, this ~~is probably~~
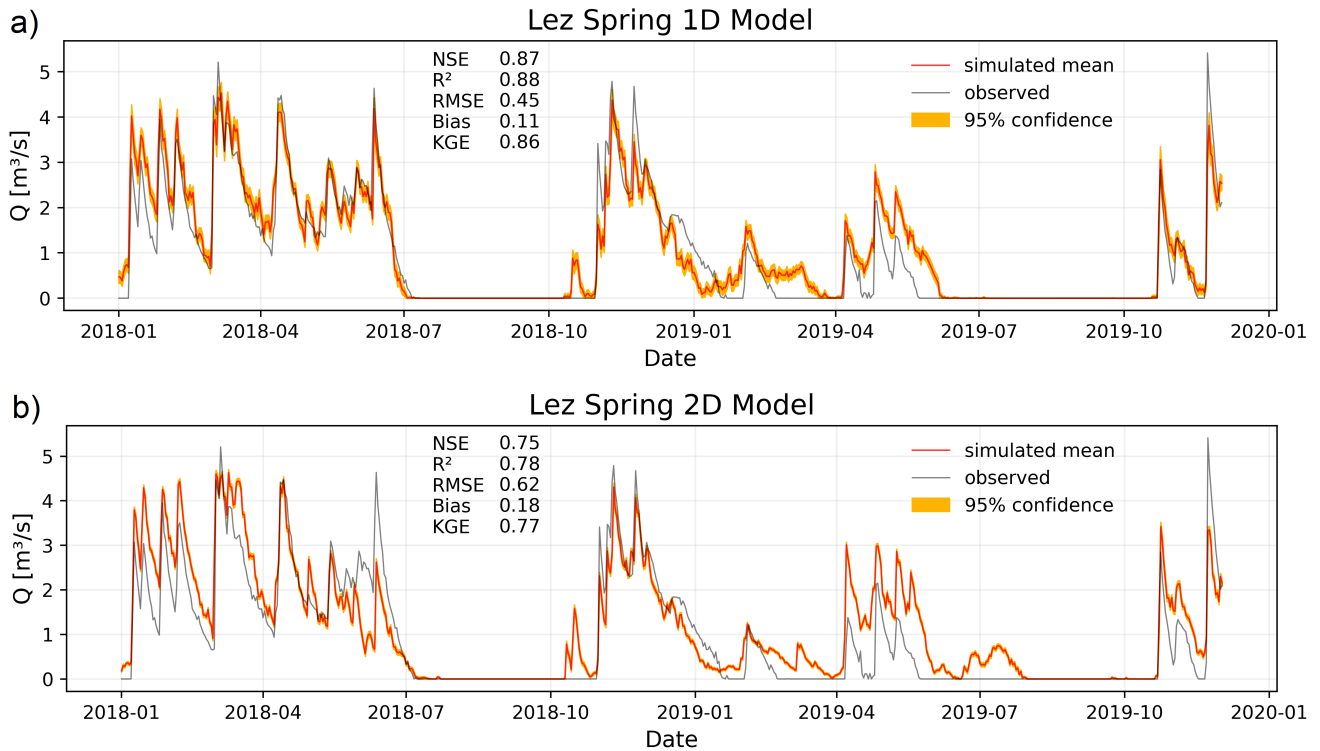
Figure 5. Simulation results for 2018-2019 at Lez spring in France using climate station input data (a) and E-OBS gridded data (b).

perfectly should be easily learnable from relative humidity and radiation data. The performance of the model is basically very
420   good, but clearly lower compared to the 1D-model, showing NSE, R^2 and KGE between 0.75 and 0.78. Generally, 2018 is
better simulated than 2019, which is however also slightly visible for the 1D-model. Some non-existent peaks are simulated
by the model in the dry sections, after all one of them (in Oct. 2018) is also simulated by the 1D-model. These Presumably,
these differences in performance can probably be explained by looking again at the input data. The climate stations, from
which the interpolated precipitation time series is derived, are mainly located inside the catchment and additionally represent a
425   good spatial coverage. Compared to both other study areas the 1D input uncertainty is definitely the best lowest for Lez spring
catchment. Though, it seems harder to extract the relevant data from the gridded data, which may be related to uncertainties
from the grid cell size in relation to the catchment size (e.g. which may be more important than for Unica but way less than
for Aubach). Nevertheless, the model uncertainty based on initializations and derived from Monte-Carlo dropout again is
satisfyingly small for both model setups, especially for the during dry periods.
430   For all study areas in this work, Lez spring is the one with the most existing modeling approaches , including several
ANN studies. Please refer to Kong A Siou et al. (2011) for an overview about older modeling studies Several other modeling
approaches exist for comparison at Lez springwith different approaches. In this study, we focus on the most recent studies for

17

~~comparison, all of which were conducted with ANNs (Kong A Siou et al., 2011, 2012; Kong-A-Siou et al., 2013, 2014; Darras et al., 2015;~~
~~. These studies are based on modeling Lez spring using Multi-Layer-Perceptrons (MLP) or recurrent MLPs. They use a wide~~
~~variation of daily data from different time periods and also have different study goals. Darras et al. (2015, 2017) focus only~~
~~on single events to evaluate flash flood forecasting. Of the other studies, especially three are suitable for a comparison with~~
~~the results of our work. Kong-A-Siou et al. (2013) uses~~ , of which we refer to three especially suited studies in the following.
Kong-A-Siou et al. (2013) used a 1-year test set in 2002-2003 and ~~obtains~~ obtained the highest NSE of all studies (0.96), however the focus of the study ~~is~~ was knowledge extraction from the ANN. Kong-A-Siou et al. (2014) ~~simulate~~ simulated the period from October 2003 to August 2004 (NSE: 0.85) and Kong-A-Siou et al. (2015) ~~investigate~~ investigated different years between 1997 and 2004 with strongly varying NSE values ranging from 0.1 to 0.85. Compared to our study, usually a larger database ~~is~~ was used for training in these studies, which in itself is a plausible reason for the good performance. ~~Also significant effort was mostly put into~~ Most studies put substantial effort into the consideration of evapotranspiration or potential evaporation, further sometimes pumping data from the accompanying wells ~~is~~ was also used as ~~input. We therefore~~ an input, which we, however, did not include due to the data availability reasons elaborated in section 2.4, as well as to be consistent in the 2D modeling approach, which would need an update of the model structure due the 1D-time series character of the pumping data. Despite limited comparability, we nevertheless can conclude that our 1D-CNN models ~~in~~ can compete with the performance of these earlier ANN approaches even though we do not beat the best NSE value from these studies ~~; however~~ due to the fact that we use less and differing input data for our 1D-model. The 2D-approach still shows very solid performance in comparison, but cannot fully compete with the 1D-model and earlier ANN approaches. Nevertheless, we also show that it ~~offers a solid alternative~~ would offer a solid substitute of the 1D-model if no climate stations were available.

4.4 Spatial Input Sensitivity Results

The most important results of the spatial input sensitivity analysis from all catchments are shown in Figure 6. In case of Aubach spring modeled with ERA5-Land data (Fig. 6a), we can see that the catchment is hardly the size of one grid cell. Hence, despite the quite solid discharge modeling, we see no clear spatial meaning of the precipitation channel heatmap but the higher sensitivity in the ~~direction the weather is approximately coming from~~ main direction of the weather area. We also see a border effect with an almost uniform decrease in sensitivity toward the edges. This is an important reason to choose the spatial extent of the data large enough, as ~~it is probably~~ this effect should be related to the size of the filter in the convolutional layer (3 x 3). This occurs even though clipping is ~~used while performing convolutions~~ applied to improve the informative value of the edges. Though, not all heatmaps show this pattern ~~. In case of Lez spring~~ (Fig. 6d) ~~we see that the sensitive region is clearly separated from the rest, thus we cannot see a border effect even if probably present~~. For Aubach spring, precipitation shows only the fourth highest sensitivity (S) in terms of absolute values, while the second most sensitive parameter is snowmelt (SMLT), which shows also the best spatial agreement with the catchment area. This is plausible insofar as the discharge for a large part of the time is dominated by snowmelt and to a lesser extent directly by precipitation. We conclude that even though the modeling results are satisfying, not much meaning can be extracted from the spatial sensitivity analysis for such a small catchment. Please find heatmaps of all other parameters in Appendix ~~C~~ Figure C1. The combined approach of RADOLAN

and ERA5-Land (Fig. 6b) data shows the heatmap in more detail in relation to the size of the catchment. We show only the precipitation heatmap, because it is the only parameter with a native resolution of 1 km x 1 km and we do not consider the spatial patterns of the remaining ERA5-Land-based parameters to be meaningful to interpret. We observe that the most sensitive cells are identified close to the spring and at the border between the main catchment and the southern adjacent subcatchment. The pronounced elongation from NW to SE ~~might be a relic from spatial correlation~~ coincides again with the main weather direction of this area. Due to the small scale of the spatial extent shown in Fig. 6b in relation to the spatial extent of precipitation events. ~~No obvious~~, the model is not able to sharpley distinguish between precipitation inside and outside the catchment. This is presumably also related to the data, as precipitation is not directly measured, but estimated from radar signals and subsequently adjusted according to measured values from nearby climate stations. It remains unclear if real world precipitation is spatially resolved with sufficient accuracy in such alpine valleys on km-scale, even though the data are undoubtful useful for modeling the absolute discharge signal. No explanation can be given for the two separate sensitive areas in the SW and NE corners, however, they are less sensitive then the center cells of the map.

Heatmaps of all four selected E-OBS parameters at Unica catchment are shown in Figure 6c. In accordance with our expectation for karst areas, we see the highest sensitivity for precipitation, which visually also identifies the catchment area ~~quite exactly. We think that the size of the Unica catchment in terms of catchment delineation is probably the best out of all three catchments investigated in this study, concerning the given spatial resolution of the used input data.~~ very well. Especially Tmax and rH show high sensitivities on larger areas, however they are usually highly spatially autocorrelated and do not show a strong spatial heterogeneity like precipitation, which makes it plausible that the model learns from larger ~~data fractions~~areas. The model further identifies an area in the north as most sensitive for radiation. ~~We know that radiation is a controlling factor for snowmelt. Thus, we can speculate that snowmelt in this northern area, which is already part of the Alps, might be well correlated to the catchment snowmelt. On catchment scale, however, more snow is expected in the southern part, which cannot be seen on the heatmap.~~

Heatmaps of the 2D-Lez spring model are shown in Figure 6d. In this area the model very strongly ignores large parts of the input data (dark blue, no visible border effects) and comparably well identifies the relevant area for the spring. This might be related to (i) the higher spatial heterogeneity of precipitation in Mediterranean climate or (ii) the lower dampening of the Lez spring karst system compared to the other study areas. Generally, we observe a slight south and east shift of the highest sensitivity compared to the catchment position. This might be related to the performance of the 2D-approach, which could not compete with the 1D-models. Maybe the model did not exactly learn the most relevant input fraction. The most sensitive parameter is precipitation, while the rH channel shows the best spatial fit. We furthermore see that the size of the catchment is about the minimum size to produce meaningful heatmaps based on this given grid resolution, which corresponds also to our interpretation of the 2D-model performance shortcomings in comparison with the 1D-approach.

Given the spatial resolution of the used input data, the obtained heatmaps, and the simulation results of all three catchments, the size of the Unica springs catchment seems to be most appropriate to investigate the usefulness for catchment localization. We conducted additional experiments to investigate the sensitivity of our approach to the absolute catchment location within the selected spatial data frame. Figure 7 shows the results of these experiments, where we shifted the 2D input data boundaries in
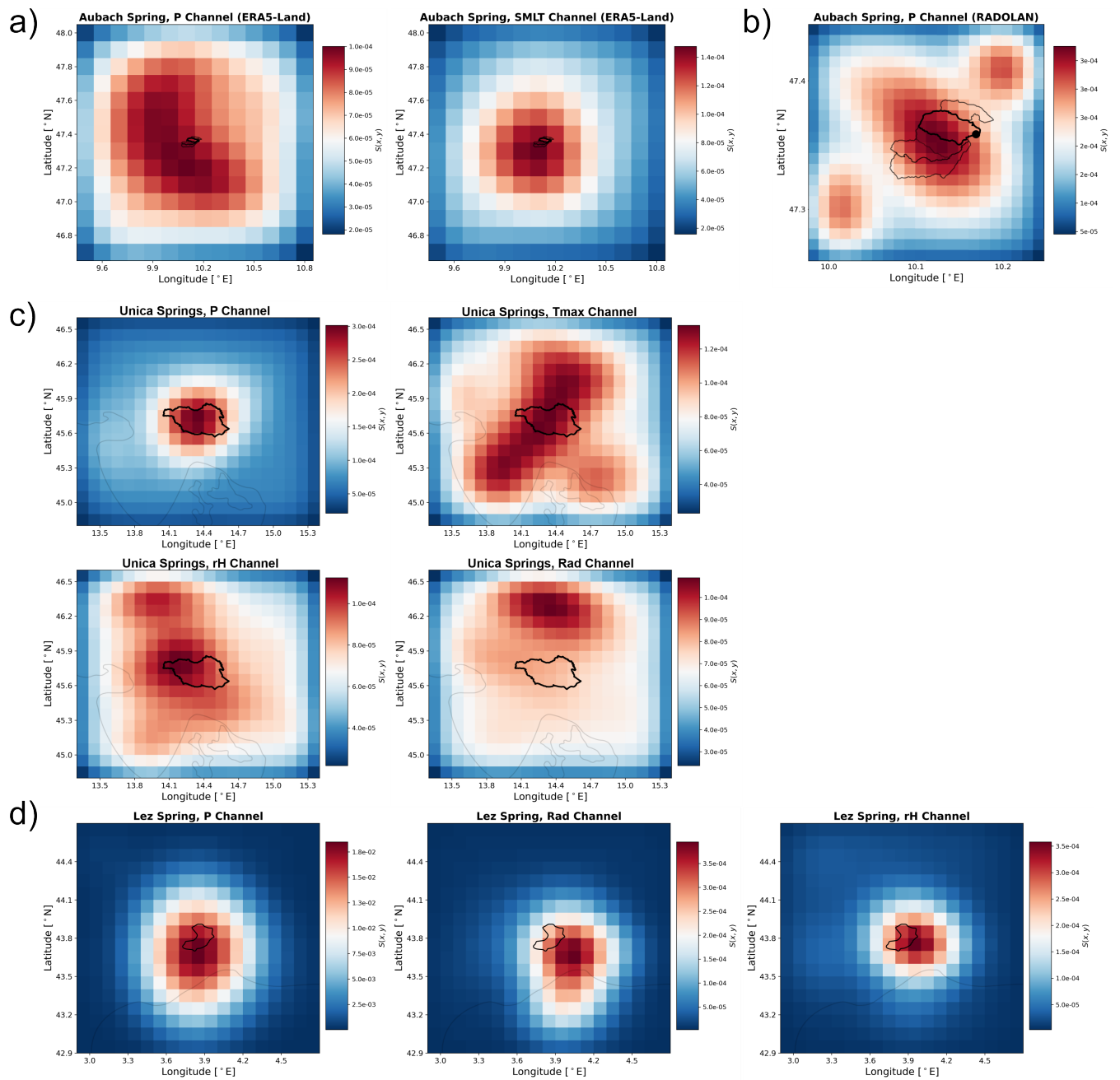
19

Figure 6. Heatmaps of spatial input sensitivity for Aubach spring based on ERA5-Land gridded data (a), for Aubach spring based on RADOLAN precipitation data (b), Unica springs (c) and Lez spring (d) both based on E-OBS gridded data. In case of (c) and (d), light-grey lines indicate the coastlines for orientation.

such a way that the catchment is located in one of the four corners or edges, leading to eight additional modeling results, named by the position of the catchment in the data frame (e.g. *upleft*: catchment in the upper left corner). First of all, we find that all models are similarly able to extract the relevant input data and thus successfully model the spring discharge curve. The NSE

505 values vary moderately between 0.80 and 0.85 among all models. Moreover, the heatmaps of the precipitation input channel visually well identify the location of the catchment for each of the different data frames used. We find that regardless of the catchment's position within the data frame, the resulting high-sensitive area in the P channel is very similar. For the heatmaps of the other input channels, we see that usually larger areas are identified as relevant and more variations between the models occur. Two things are particularly noticeable here. First, the identified sensitive input areas are generally slightly smaller for the

510 *up** models, which is possibly related to the fact that the data frame is shifted towards the Mediterranean Sea, where no input data are available in the E-OBS dataset (compare the grey coastline). These areas contain zeros or mean values and show no temporal variation that could be used to model the spring discharge. Second, the noticeably best performing model (*downleft*, NSE of 0.85) is the model with the least fraction of no-data cells (due to the Sea) in the data frame. Intuitively, we would not have expected the best performance here, but rather with the *upright* model, since there it is almost predetermined where

515 the model has to learn. So the model seems to be able to use the larger amount of "useful data", even outside the catchment, to improve the overall performance. To possibly delineate a catchment from these results, a strategy has to be developed regarding the sensitivity contrast between the catchment and its surroundings. From our results we conclude that focusing on the precipitation channel is the most promising approach for potential catchment delineation. This makes, however, only sense if (i) precipitation is sufficiently heterogeneous at the scale of investigation, and (ii) if conceptually spring discharge is mainly

520 driven by precipitation (not snowmelt for example). Please find the precipitation channel heatmaps for Aubach spring and Lez spring in Appendix Figures C2 and C3.

In summary, we observe that the approach in its current form can produce meaningful heatmaps for at least roughly locating karst spring catchments. At least for the precipitation channel, we showed that the location of the catchment is successfully learned, regardless of the position within the selected spatial data frame, if the ratio of catchment size to grid cell size is

525 favorable (as for Unica springs). We notice that it generally works better the larger the catchment area, especially in relation to the grid cell size, but the absolute size of the catchment itself appears to be also important. For small catchments it seems harder to extract precise catchment locations, even if spatially finer-resolved data are available. This might be related to the fact that at small scales, even precipitation has a distinct spatial correlation, which can lead to higher sensitivity also in areas outside the catchment. However, one should keep in mind that these conclusions are only tendencies as we only investigated a small

530 number of catchments. To develop a catchment delineation strategy, future investigations should analyze more catchments with adequate ratio of size to grid cell resolution, such as Unica catchment. Moreover, it can be expected that more and better gridded meteorological data products will be available in the future, which might lead to better results with the proposed methodology also for catchments with varying sizes.
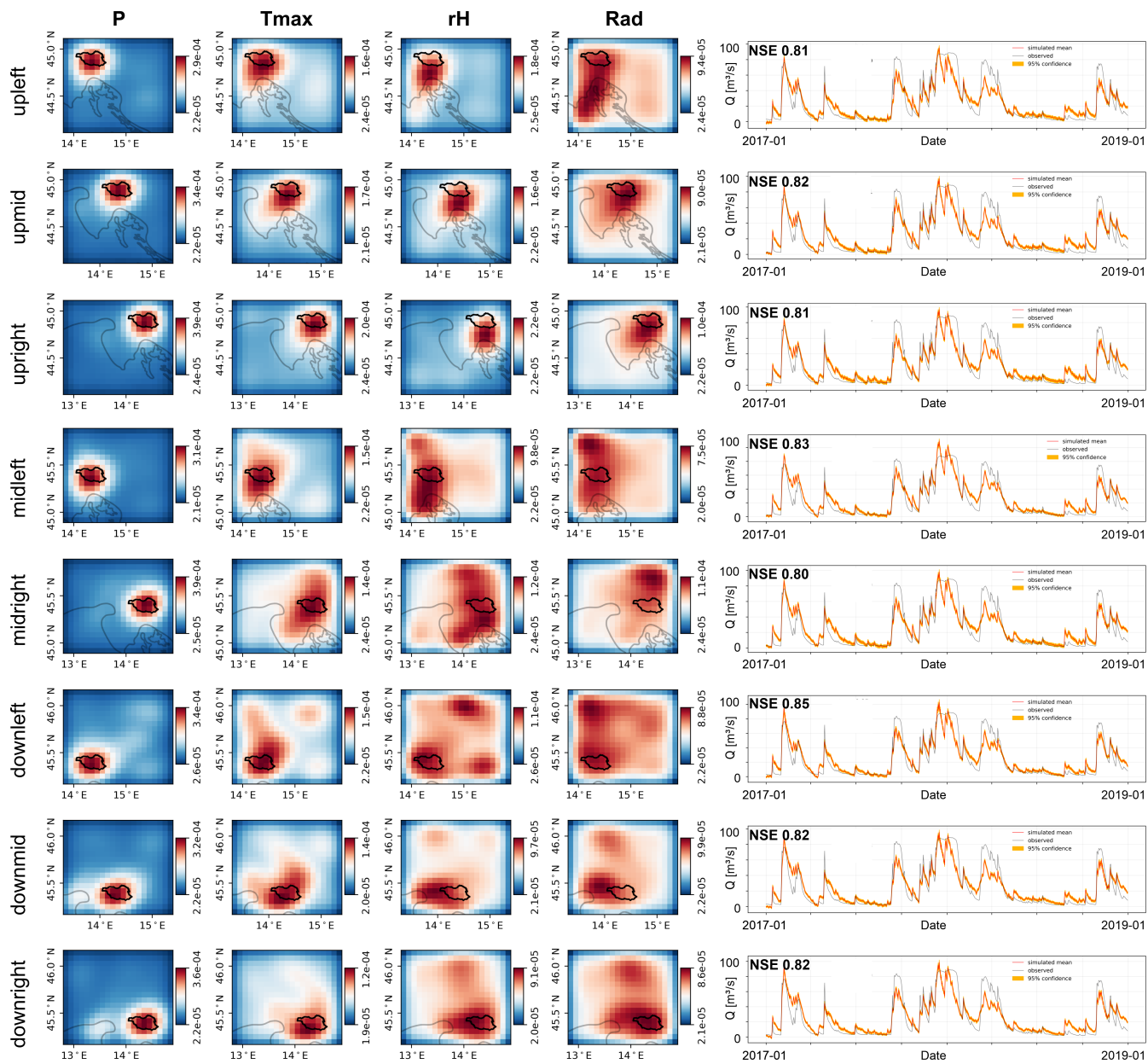
Figure 7. Heatmaps of spatial input sensitivity for Unica springs catchment based on E-OBS gridded data. The gridded data section is shifted to demonstrate the spatial learning capabilities of the models.

5   Conclusions

From the obtained insights we can conclude that karst spring discharge can be predicted accurately with the presented 1D and 2D approaches. Their accuracy rivals that of existing models in the three study areas, with the difference that far less prior knowledge of the system under consideration is required than, e.g., for lumped parameter models. This can ~~significantly~~ substantially reduce the amount of work required, provided that a mere simulation of the spring discharge is the objective~~; albeit, we do not gain knowledge about hydraulic processes in the aquifer as we do from lumped parameter models~~. We can further show that gridded climate data can provide an excellent substitute for non-existent or patchy climate station data. This does not require knowledge of the exact catchment area, which is a critical component especially for karst springs. Rather, 2D-CNNs can be used to generate a first approximation of the catchment ~~area~~location. However, this approach is subject to some inaccuracies and needs further development in combination with 2D-meteorological input data in a finer spatial resolution in relation to the catchment size. Additionally, a sufficient heterogeneity of precipitation in comparison to the catchment size is necessary. Then~~it can most certainly~~, we assume it can be used to delineate catchments quite accurately, which can then be evaluated against tracer tests and hydrogeological studies. In ~~the present state, however, it does not replace conventional catchment delineation methods. In~~ terms of accuracy, we do not find that one of the tested model setups is fundamentally superior. Nevertheless, we would conclude that the 2D-approach is superior to the 1D-approach with respect to the effort of data collection as well as data and parameter availability. Though, a ~~significantly~~ substantially increased computational effort is necessary for the training as well as for the optimization of the models. In summary, gridded meteorological data is excellently useful to overcome missing climate station data and to get a quite good idea of the spatial extent of larger catchments in relation to the grid cell size.

Appendix A: Study Area Comparison Table

Table A1. Summary and comparison of different aspects of all three study areas.

	Aubach Spring	Unica Springs	Lez Springs
Country	Austria	Slovenia	France
Climate	cooltemperate and humid	moderate continental	mediterranean
Catchment Area [km^2]	9	820	240
mean Precipitation [mm/year]	2000	1500	904
Station, Period	(Walm.-Horn, 2003-2019)	(1989-2018)	(2008-2018)
spatially distributed input datasets	ERA5-Land, RADOLAN	E-OBS	E-OBS
Offered Parameters	P, T, Tsin, E, SMLT, SF, SWVL1-4	P, T, Tmin, Tmax, Tsin, rH, Rad	P, T, Tmin, Tmax, Tsin, rH, Rad
Selected Parameters	ERA5-Model: P, T, E, SMLT, SWVL2, 4 RADOLAN-Model: P, T, Tsin, SMLT, SF, SWVL1, 2, 4	P, Tmax, rH, Rad	P, rH, Rad
Omitted Parameters	ERA5-Model: Tsin, SF, SWVL1, 3 RADOLAN-Model: E, SWVL3	T, Tmin, Tsin	T, Tmin, Tmax, Tsin

Appendix B: Lez Catchment Precipitation Interpolation

The Thiessen's polygon interpolation method consists of calculating a weighted average of the precipitation data by allocating a contribution percentage to each meteorological station, based on its influence area on the catchment. These influence areas are calculated through geometric operations. First, we draw straight-line segments between each adjacent station, then we add the perpendicular bisectors of each segment, which will define the edges of the polygons. Each meteorological station thus corresponds to a particular polygon, for which the precipitation over the surface is assumed to be the same as the measured precipitation at the station.

The weighted average of the precipitation P_{wa} at each time step is calculated as follows:

$$P_{wa} = \frac{\sum_{i=1}^{n} A_i P_i}{A} \tag{B1}$$

With n the number of meteorological stations, A_i the area (over the catchment) of the polygon corresponding to the ith station, P_i the precipitation measured at the ith station and A the area of the catchment.
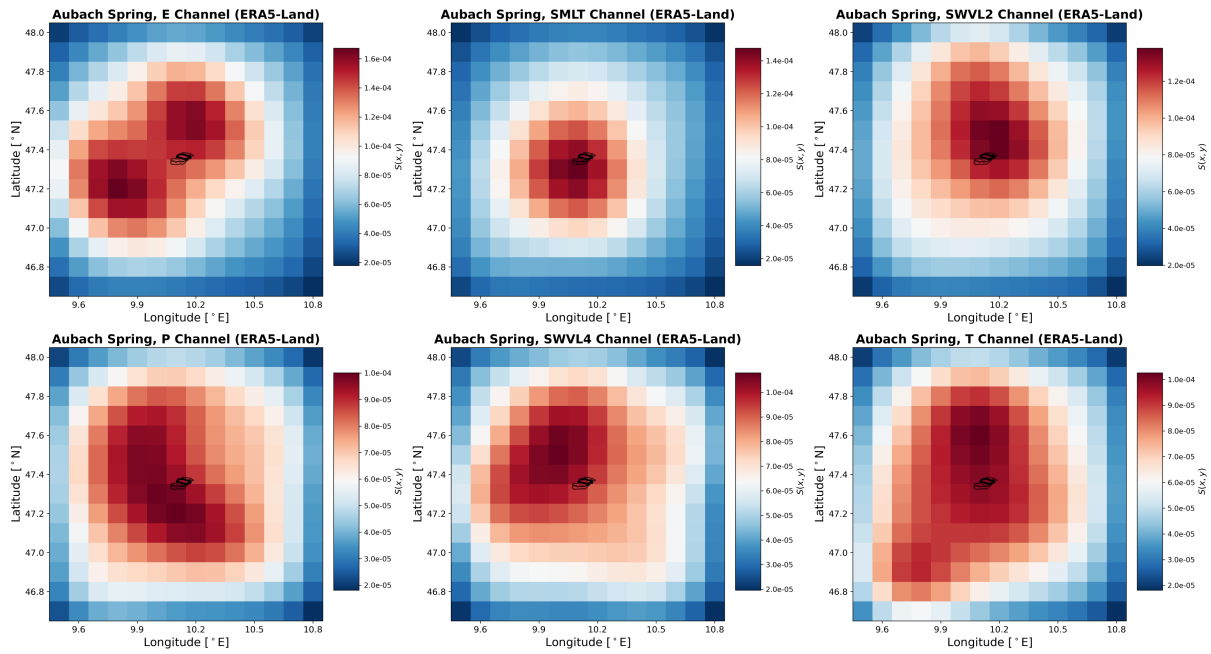
Appendix C: Heatmaps

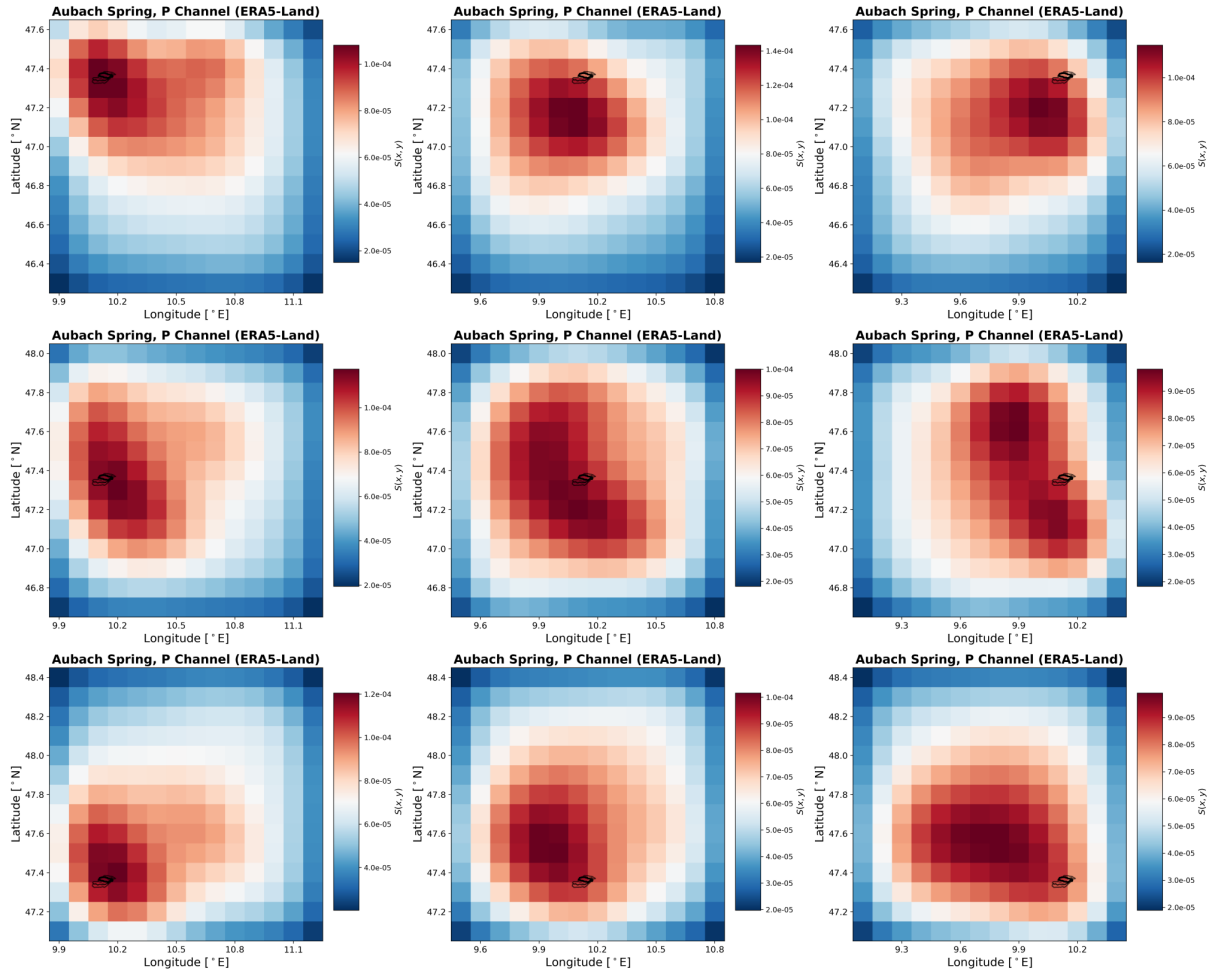**Figure C1.** Spatial input sensitivity heatmaps for Aubach spring based on ERA5-Land gridded data.

Figure C2. P-channel heatmaps based on ERA5-Land gridded data for Aubach spring with shifted spatial data frame in relation to the catchment position.
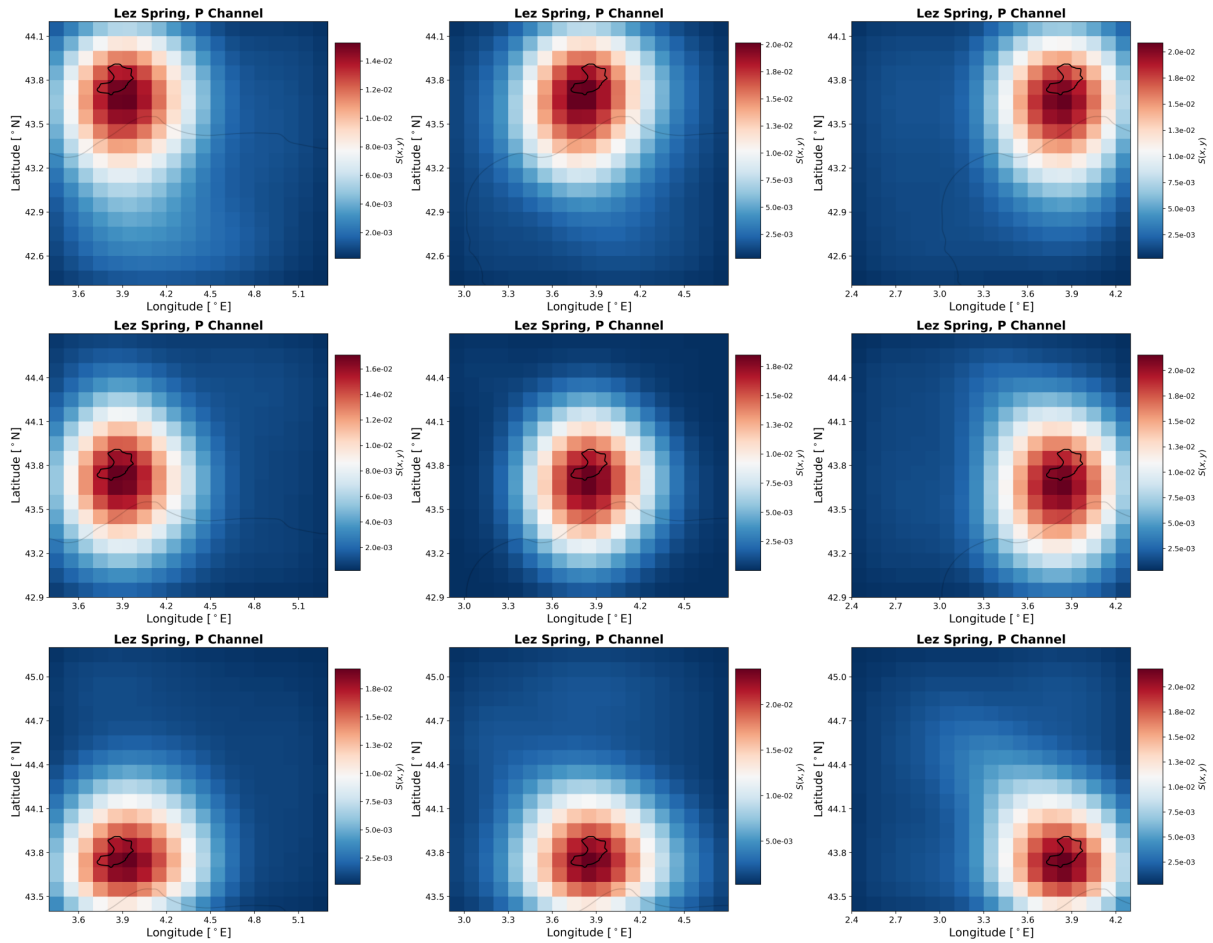
Figure C3. P-channel heatmaps based on E-OBS gridded data for Lez spring with shifted spatial data frame in relation to the catchment position.

Appendix D: Model Overview

Table D1. Model parameter summary table.

Optimized Hyperparamaters	Aubach (ERA5)	Aubach (RADOLAN)	Lez	Unica
n (1DConv filter)	128	128	16	16
input seq. length	54 (hours)	162 (hours)	53 (days)	40 (days)
batch-size	64	256	32	32
Other Hyperparameters				
inital learning rate	0.001	0.001	0.001	0.001
training epochs	100	100	100	100
early stopping patience	12	8	12	12
Model Summaries				
total parameters	708,353	1,502,849	358,977	384,017
trainable par.	708,097	1,502,593	358,945	383,985
non-trainable par.	256	256	32	32

Author contributions. AW, TL and NG conceptualized the study, AW and TL developed the methodology and software code, and validated the results. AW performed the experiments, and investigated and visualized the results. GC and ZC performed formal analysis, NR and GC contributed to data curation activities. AW wrote the original paper draft with contributions from GC and NR. All authors contributed to interpretation of the results, and review and editing of the paper draft. TL and NG supervised the work.

References

Abadi, M., Agarwal, A., Barham, P., Brevdo, E., Chen, Z., Citro, C., Corrado, G. S., Davis, A., Dean, J., Devin, M., Ghemawat, S., Good-
fellow, I., Harp, A., Irving, G., Isard, M., Jia, Y., Jozefowicz, R., Kaiser, L., Kudlur, M., Levenberg, J., Mane, D., Monga, R., Moore, S.,
Murray, D., Olah, C., Schuster, M., Shlens, J., Steiner, B., Sutskever, I., Talwar, K., Tucker, P., Vanhoucke, V., Vasudevan, V., Viegas, F.,
Vinyals, O., Warden, P., Wattenberg, M., Wicke, M., Yu, Y., and Zheng, X.: TensorFlow: Large-Scale Machine Learning on Heterogeneous
Distributed Systems, p. 19, https://www.tensorflow.org/, 2015.

Afzaal, H., Farooque, A. A., Abbas, F., Acharya, B., and Esau, T.: Groundwater Estimation from Major Physical Hydrology Components
Using Artificial Neural Networks and Deep Learning, Water, 12, 5, https://doi.org/10.3390/w12010005, 2020.

Anderson, S. and Radic, V.: Evaluation and Interpretation of Convolutional-Recurrent Networks for Regional Hydrological Modelling,
Hydrology and Earth System Sciences Discussions, 2021, 1–43, https://doi.org/10.5194/hess-2021-113, 2021.

ARSO: Slovenian Environment Agency. Archive of Hydrological Data., http://vode.arso.gov.si/hidarhiv/, 2020a.

ARSO: Slovenian Environment Agency. Archive of Meteorological Data., http://www.meteo.si, 2020b.

Bergström, S.: The Development of a Snow Routine for the HBV-2 Model, Hydrology Research, 6, 73–92, https://doi.org/10/gkcqz5, 1975.

Bergström, S.: The HBV Model, in: Computer Models of Watershed Hydrology., edited by Singh, V. P., pp. 443–476, Water Resources
Publications, Colorado, USA, https://www.cabdirect.org/cabdirect/abstract/19961904773, 1995.

Bicalho, C. C., Batiot-Guilhe, C., Seidel, J. L., Van Exter, S., and Jourde, H.: Hydrodynamical Changes and Their Consequences on Ground-
water Hydrochemistry Induced by Three Decades of Intense Exploitation in a Mediterranean Karst System, Environ Earth Sci, 65, 2311–
2319, https://doi.org/10.1007/s12665-011-1384-2, 2012.

Chen, Z. and Goldscheider, N.: Modeling Spatially and Temporally Varied Hydraulic Behavior of a Folded Karst Sys-
tem with Dominant Conduit Drainage at Catchment Scale, Hochifen–Gottesacker, Alps, Journal of Hydrology, 514, 41–52,
https://doi.org/10.1016/j.jhydrol.2014.04.005, 2014.

Chen, Z., Auler, A. S., Bakalowicz, M., Drew, D., Griger, F., Hartmann, J., Jiang, G., Moosdorf, N., Richts, A., Stevanovic, Z., Veni, G.,
and Goldscheider, N.: The World Karst Aquifer Mapping Project: Concept, Mapping Procedure and Map of Europe, Hydrogeol J, 25,
771–785, https://doi.org/10/f98h6g, 2017a.

Chen, Z., Hartmann, A., and Goldscheider, N.: A New Approach to Evaluate Spatiotemporal Dynamics of Controlling Parameters in Dis-
tributed Environmental Models, Environmental Modelling & Software, 87, 1–16, https://doi.org/10.1016/j.envsoft.2016.10.005, 2017b.

Chen, Z., Hartmann, A., Wagener, T., and Goldscheider, N.: Dynamics of Water Fluxes and Storages in an Alpine Karst Catchment under
Current and Potential Future Climate Conditions, Hydrol. Earth Syst. Sci., p. 17, https://doi.org/10.5194/hess-22-3807-2018, 2018.

Chollet, F.: Keras, https://github.com/keras-team/keras, 2015.

Cornes, R. C., van der Schrier, G., van den Besselaar, E. J. M., and Jones, P. D.: An Ensemble Version of the E-OBS Temperature and
Precipitation Data Sets, J. Geophys. Res. Atmos., 123, 9391–9409, https://doi.org/10/gfk3hd, 2018.

Darras, T., Borrell Estupina, V., Kong-A-Siou, L., Vayssade, B., Johannet, A., and Pistre, S.: Identification of Spatial and Temporal Contri-
butions of Rainfalls to Flash Floods Using Neural Network Modelling: Case Study on the Lez Basin (Southern France), Hydrology and
Earth System Sciences, 19, 4397–4410, https://doi.org/10/f7xq6q, 2015.

Darras, T., Kong-A-Siou, L., Vayssade, B., Johannet, A., and Pistre, S.: Karst Flash Flood Forecasting Using Recurrent and Nonrecurrent
Artificial Neural Network Models: The Case of the Lez Basin (Southern France), in: EuroKarst 2016, Neuchâtel, Advances in Karst
Science, Springer International Publishing, Cham, https://doi.org/10.1007/978-3-319-45465-8, 2017.

630   DWD Climate Data Center (CDC): Historical and Current Hourly RADOLAN Grids of Precipitation Depth (Binary). Version V001, https://opendata.dwd.de/climate_environment/CDC/grids_germany/hourly/radolan/.

Fleury, P., Ladouche, B., Conroux, Y., Jourde, H., and Dörfliger, N.: Modelling the Hydrologic Functions of a Karst Aquifer under Active Water Management – The Lez Spring, Journal of Hydrology, 365, 235–243, https://doi.org/10.1016/j.jhydrol.2008.11.037, 2009.

Goldscheider, N.: Fold Structure and Underground Drainage Pattern in the Alpine Karst System Hochifen-Gottesacker, Eclogae geol. Helv.,
635   98, 1–17, https://doi.org/10.1007/s00015-005-1143-z, 2005.

Gupta, H. V., Kling, H., Yilmaz, K. K., and Martinez, G. F.: Decomposition of the Mean Squared Error and NSE Performance Criteria: Implications for Improving Hydrological Modelling, Journal of Hydrology, 377, 80–91, https://doi.org/10.1016/j.jhydrol.2009.08.003, 2009.

Hock, R.: A Distributed Temperature-Index Ice- and Snowmelt Model Including Potential Direct Solar Radiation, Journal of Glaciology, 45,
640   101–111, https://doi.org/10/ggnvkt, 1999.

Hunter, J. D.: Matplotlib: A 2D Graphics Environment, Computing in Science Engineering, 9, 90–95, https://doi.org/10.1109/mcse.2007.55, 2007.

Hussain, D., Hussain, T., Khan, A. A., Naqvi, S. A. A., and Jamil, A.: A Deep Learning Approach for Hydrological Time-Series Prediction: A Case Study of Gilgit River Basin, Earth Sci Inform, 13, 915–927, https://doi.org/10/gnc9d5, 2020.

645   Ioffe, S. and Szegedy, C.: Batch Normalization: Accelerating Deep Network Training by Reducing Internal Covariate Shift, arXiv:1502.03167 [cs], http://arxiv.org/abs/1502.03167, 2015.

Jeannin, P.-Y., Artigue, G., Butscher, C., Chang, Y., Charlier, J.-B., Duran, L., Gill, L., Hartmann, A., Johannet, A., Jourde, H., Kavousi, A., Liesch, T., Liu, Y., Lüthi, M., Malard, A., Mazzilli, N., Pardo-Igúzquiza, E., Thiéry, D., Reimann, T., Schuler, P., Wöhling, T., and Wunsch, A.: Karst Modelling Challenge 1: Results of Hydrological Modelling, Journal of Hydrology, 600, 126 508,
650   https://doi.org/10.1016/j.jhydrol.2021.126508, 2021.

Johannet, A., Mangin, A., and D'Hulst, D.: Subterranean Water Infiltration Modelling by Neural Networks: Use of Water Source Flow, in: ICANN '94: Proceedings of the International Conference on Artificial Neural Networks Sorrento, Italy, 26–29 May 1994 Volume 1, Parts 1 and 2, pp. 1033–1036, Springer Berlin Heidelberg, Sorrento, Italy, 1994.

Jourde, H., Lafare, A., Mazzilli, N., Belaud, G., Neppel, L., Dörfliger, N., and Cernesson, F.: Flash Flood Mitigation as a Posi-
655   tive Consequence of Anthropogenic Forcing on the Groundwater Resource in a Karst Catchment, Environ Earth Sci, 71, 573–583, https://doi.org/10.1007/s12665-013-2678-3, 2014.

Jourde, H., Massei, N., Mazzilli, N., Binet, S., Batiot-Guilhe, C., Labat, D., Steinmann, M., Bailly-Comte, V., Seidel, J. L., Arfib, B., Charlier, J. B., Guinot, V., Jardani, A., Fournier, M., Aliouache, M., Babic, M., Bertrand, C., Brunet, P., Boyer, J. F., Bricquet, J. P., Camboulive, T., Carrière, S. D., Celle-Jeanton, H., Chalikakis, K., Chen, N., Cholet, C., Clauzon, V., Soglio, L. D., Danquigny, C., Défargue, C., Denimal,
660   S., Emblanch, C., Hernandez, F., Gillon, M., Gutierrez, A., Sanchez, L. H., Hery, M., Houillon, N., Johannet, A., Jouves, J., Jozja, N., Ladouche, B., Leonardi, V., Lorette, G., Loup, C., Marchand, P., de Montety, V., Muller, R., Ollivier, C., Sivelle, V., Lastennet, R., Lecoq, N., Maréchal, J. C., Perotin, L., Perrin, J., Petre, M. A., Peyraube, N., Pistre, S., Plagnes, V., Probst, A., Probst, J. L., Simler, R., Stefani, V., Valdes-Lao, D., Viseur, S., and Wang, X.: SNO KARST: A French Network of Observatories for the Multidisciplinary Study of Critical Zone Processes in Karst Watersheds and Aquifers, Vadose Zone Journal, 17, 180 094, https://doi.org/10/gk9t3n, 2018.

665   Kaufman, G., Mayaud, C., Kogovšek, B., and Gabrovšek, F.: Understanding the Temporal Variation of Flow Direction in a Complex Karst System (Planinska Jama, Slovenia), Acta Carsologica, 49, https://doi.org/10/gkcs9h, 2020.

Kaufmann, G., Gabrovšek, F., and Turk, J.: Modelling Flow of Subterranean Pivka River in Postojnska Jama, Slovenia, Acta Carsologica, 45, https://doi.org/10.3986/ac.v45i1.3059, 2016.

Kollat, J. B., Reed, P. M., and Wagener, T.: When Are Multiobjective Calibration Trade-Offs in Hydrologic Models Meaningful?, Water
670   Resources Research, 48, https://doi.org/10/gkcq5k, 2012.

Kong A Siou, L., Johannet, A., Borrell, V., and Pistre, S.: Complexity Selection of a Neural Network Model for Karst Flood Forecasting: The Case of the Lez Basin (Southern France), Journal of Hydrology, 403, 367–380, https://doi.org/10.1016/j.jhydrol.2011.04.015, 2011.

Kong A Siou, L., Johannet, A., Valérie, B. E., and Pistre, S.: Optimization of the Generalization Capability for Rainfall–Runoff Modeling by Neural Networks: The Case of the Lez Aquifer (Southern France), Environmental Earth Sciences, 65, 2365–2375,
675   https://doi.org/10.1007/s12665-011-1450-9, 2012.

Kong-A-Siou, L., Cros, K., Johannet, A., Borrell-Estupina, V., and Pistre, S.: KnoX Method, or Knowledge eXtraction from Neural Network Model. Case Study on the Lez Karst Aquifer (Southern France), Journal of Hydrology, 507, 19–32, https://doi.org/10.1016/j.jhydrol.2013.10.011, 2013.

Kong-A-Siou, L., Fleury, P., Johannet, A., Borrell Estupina, V., Pistre, S., and Dörfliger, N.: Performance and Complementarity of Two
680   Systemic Models (Reservoir and Neural Networks) Used to Simulate Spring Discharge and Piezometry for a Karst Aquifer, Journal of Hydrology, 519, 3178–3192, https://doi.org/10.1016/j.jhydrol.2014.10.041, 2014.

Kong-A-Siou, L., Johannet, A., Borrell Estupina, V., and Pistre, S.: Neural Networks for Karst Groundwater Management: Case of the Lez Spring (Southern France), Environmental Earth Sciences, 74, 7617–7632, https://doi.org/10.1007/s12665-015-4708-9, 2015.

Kovačič, G., Petrič, M., and Ravbar, N.: Evaluation and Quantification of the Effects of Climate and Vegetation Cover Change on Karst
685   Water Sources: Case Studies of Two Springs in South-Western Slovenia, Water, 12, 3087, https://doi.org/10/gksnmz, 2020.

Lähivaara, T., Malehmir, A., Pasanen, A., Kärkkäinen, L., Huttunen, J. M. J., and Hesthaven, J. S.: Estimation of Groundwater Storage from Seismic Data Using Deep Learning, Geophysical Prospecting, 67, 2115–2126, https://doi.org/10.1111/1365-2478.12831, 2019.

Lebigot, E. O.: Uncertainties: A Python Package for Calculations with Uncertainties, https://pythonhosted.org/uncertainties/numpy_guide. html, 2010.

690 LeCun, Y., Bengio, Y., and Hinton, G.: Deep Learning, Nature, 521, 436–444, https://doi.org/10.1038/nature14539, 2015.

Longenecker, J., Bechtel, T., Chen, Z., Goldscheider, N., Liesch, T., and Walter, R.: Correlating Global Precipitation Measurement Satellite Data with Karst Spring Hydrographs for Rapid Catchment Delineation, Geophysical Research Letters, 44, 4926–4932, https://doi.org/10.1002/2017GL073790, 2017.

Maier, H. R. and Dandy, G. C.: Neural Networks for the Prediction and Forecasting of Water Resources Variables: A Review of Modelling
695   Issues and Applications, Environmental modelling & software, 15, 101–124, https://doi.org/10.1016/s1364-8152(99)00007-9, 2000.

Maier, H. R., Jain, A., Dandy, G. C., and Sudheer, K.: Methods Used for the Development of Neural Networks for the Prediction of Water Resource Variables in River Systems: Current Status and Future Directions, Environmental Modelling & Software, 25, 891–909, https://doi.org/10.1016/j.envsoft.2010.02.003, 2010.

Malard, A., Jeannin, P.-Y., Vouillamoz, J., and Weber, E.: An Integrated Approach for Catchment Delineation and Conduit-Network Modeling
700   in Karst Aquifers: Application to a Site in the Swiss Tabular Jura, Hydrogeol J, 23, 1341–1357, https://doi.org/10.1007/s10040-015-1287-5, 2015.

Mayaud, C., Gabrovšek, F., Blatnik, M., Kogovšek, B., Petrič, M., and Ravbar, N.: Understanding Flooding in Poljes: A Modelling Perspective, Journal of Hydrology, 575, 874–889, https://doi.org/10.1016/j.jhydrol.2019.04.092, 2019.

32

Mazzilli, N., Jourde, H., Guinot, V., Bailly-Comte, V., and Fleury, P.: Hydrological Modelling of a Karst Aquifer under Active Groundwater Management Using a Parsimonious Conceptual Model, in: H2Karst, Besançon, France, https://hal.archives-ouvertes.fr/hal-01844603, 2011.

McKinney, W.: Data Structures for Statistical Computing in Python, in: Python in Science Conference, pp. 56–61, Austin, Texas, https://doi.org/10.25080/majora-92bf1922-00a, 2010.

Müller, J., Park, J., Sahu, R., Varadharajan, C., Arora, B., Faybishenko, B., and Agarwal, D.: Surrogate Optimization of Deep Neural Networks for Groundwater Predictions, J Glob Optim, https://doi.org/10.1007/s10898-020-00912-0, 2020.

Muñoz Sabater, J.: ERA5-Land Hourly Data from 2001 to Present. Copernicus Climate Change Service (C3S) Climate Data Store (CDS)., https://doi.org/10.24381/CDS.E2161BAC, 2019.

NASA: GPM - Global Precipitation Measurement, http://www.nasa.gov/mission_pages/GPM/main/index.html, 2016.

Nash, J. E. and Sutcliffe, J. V.: River Flow Forecasting through Conceptual Models Part I—A Discussion of Principles, Journal of hydrology, 10, 282–290, https://doi.org/10.1016/0022-1694(70)90255-6, 1970.

Nogueira, F.: Bayesian Optimization: Open Source Constrained Global Optimization Tool for Python, https://github.com/fmfn/BayesianOptimization, 2014.

Pedregosa, F., Varoquaux, G., Gramfort, A., Michel, V., Thirion, B., Grisel, O., Blondel, M., Prettenhofer, P., Weiss, R., Dubourg, V., Vanderplas, J., Passos, A., and Cournapeau, D.: Scikit-Learn: Machine Learning in Python, Journal of Machine Learning Research, 12, 2825–2830, 2011.

Petrič, M., Kogovšek, J., and Ravbar, N.: Effects of the Vadose Zone on Groundwater Flow and Solute Transport Characteristics in Mountainous Karst Aquifers – the Case of the Javorniki–Snežnik Massif (SW Slovenia), AC, 47, https://doi.org/10.3986/ac.v47i1.5144, 2018.

Petsiuk, V., Das, A., and Saenko, K.: RISE: Randomized Input Sampling for Explanation of Black-Box Models, arXiv:1806.07421 [cs], http://arxiv.org/abs/1806.07421, 2018.

Rajaee, T., Ebrahimi, H., and Nourani, V.: A Review of the Artificial Intelligence Methods in Groundwater Level Modeling, Journal of Hydrology, 572, 336–351, https://doi.org/10.1016/j.jhydrol.2018.12.037, 2019.

Reback, J., McKinney, W., Jbrockmendel, Bossche, J. V. D., Augspurger, T., Cloud, P., Gfyoung, Sinhrks, Klein, A., Roeschke, M., Hawkins, S., Tratner, J., She, C., Ayd, W., Petersen, T., Garcia, M., Schendel, J., Hayden, A., MomIsBestFriend, Jancauskas, V., Battiston, P., Seabold, S., Chris-B1, H-Vetinari, Hoyer, S., Overmeire, W., Alimcmaster1, Dong, K., Whelan, C., and Mehyar, M.: Pandas-Dev/Pandas: Pandas 1.0.3, Zenodo, https://doi.org/10.5281/ZENODO.3509134, 2020.

Seibert, J.: Multi-Criteria Calibration of a Conceptual Runoff Model Using a Genetic Algorithm, Hydrology and Earth System Sciences, 4, 215–224, https://doi.org/10/crmzd7, 2000.

Sezen, C., Bezak, N., Bai, Y., and Šraj, M.: Hydrological Modelling of Karst Catchment Using Lumped Conceptual and Data Mining Models, Journal of Hydrology, 576, 98–110, https://doi.org/10.1016/j.jhydrol.2019.06.036, 2019.

Sit, M., Demiray, B. Z., Xiang, Z., Ewing, G. J., Sermet, Y., and Demir, I.: A Comprehensive Review of Deep Learning Applications in Hydrology and Water Resources, Water Science and Technology, 82, 2635–2670, https://doi.org/10/ghwnnk, 2020.

SNO KARST: Time Series of Type Hydrology-Hydrogeology in Le Lez (Méditerranée) Basin - MEDYCYSS Observatory - KARST Observatory Network - OZCAR Critical Zone Network Research Infrastructure, https://doi.org/10.15148/CFD01A5B-B7FD-41AA-8884-84DBDDAC767E, 2021.

Srivastava, N., Hinton, G., Krizhevsky, A., Sutskever, I., and Salakhutdinov, R.: Dropout: A Simple Way to Prevent Neural Networks from Overfitting, Journal of Machine Learning Research, 15, 1929–1958, http://jmlr.org/papers/v15/srivastava14a.html, 2014.

Stevanović, Z.: Karst Waters in Potable Water Supply: A Global Scale Overview, Environ Earth Sci, 78, 662, https://doi.org/10.1007/s12665-019-8670-9, 2019.

Thiéry, D. and Bérard, P.: Alimentation en eau de la ville de Montpellier - captage de la source du Lez - études des relations entre la source
745   et son réservoir aquifère, Tech. rep., BRGM No. 83, SNG 167 LRO, http://infoterre.brgm.fr/rapports/83-SGN-167-LRO.pdf, 1983.

Van, S. P., Le, H. M., Thanh, D. V., Dang, T. D., Loc, H. H., and Anh, D. T.: Deep Learning Convolutional Neural Network in Rainfall–Runoff
Modelling, Journal of Hydroinformatics, 22, 541–561, https://doi.org/10.2166/hydro.2020.095, 2020.

van der Walt, S., Colbert, S. C., and Varoquaux, G.: The NumPy Array: A Structure for Efficient Numerical Computation, Comput. Sci. Eng.,
13, 22–30, https://doi.org/10.1109/mcse.2011.37, 2011.

750   van Rossum, G.: Python Tutorial, 1995.

Wunsch, A.: AndreasWunsch/CNN_KarstSpringModeling, GitHub repository, Zenodo, https://github.com/AndreasWunsch/CNN_KarstSpringModeling, 2021.

Wunsch, A., Liesch, T., and Broda, S.: Groundwater Level Forecasting with Artificial Neural Networks: A Comparison of Long Short-Term
Memory (LSTM), Convolutional Neural Networks (CNNs), and Non-Linear Autoregressive Networks with Exogenous Input (NARX),
755   Hydrology and Earth System Sciences, 25, 1671–1687, https://doi.org/10.5194/hess-25-1671-2021, 2021.

Zeiler, M. D. and Fergus, R.: Visualizing and Understanding Convolutional Networks, in: Computer Vision – ECCV 2014, edited by Fleet,
D., Pajdla, T., Schiele, B., and Tuytelaars, T., pp. 818–833, Springer International Publishing, Cham, 2014.